POLITECNICO DI TORINO

Master's Degree Course in Mechanical Engineering

MASTER'S DEGREE THESIS

Pyroshock Testing of a Resonant Plate Using Hammer Impact

Advisor

Prof. DAGA ALESSANDRO PAOLO

Co- advisors:

Doc. VIALE LUCA

Candidate:

CHEN ZHIYONG

June 2023

Abstract

Pyroshock is the high-frequency, high-amplitude shock generated during the separation stage of launch of aerospace vehicles. While undergoing pyroshock, structural and electronic equipment may be subjected to the impact waves caused by the explosion, leading to damage, malfunction, or failure of the devices [4]. The purpose of conducting pyroshock testing is to evaluate whether structural or electronic equipment can function properly in real pyroshock environments. Pyroshock tests are typically conducted in simulated environments to generate controlled shock waveforms and spectra that resemble actual pyroshock events. Through pyroshock testing, the performance and reliability of aerospace equipment can be assessed, ensuring their ability to operate smoothly and successfully complete missions in real-world scenarios [1].

Due to the cost and hazards associated with pyrotechnic devices, mechanical pyroshock simulation devices can be used for pyroshock testing. In this study, a hammer's impact device was used to simulate pyroshock, and specific variables were selected to study the impact force. In particular, the focus was on the mass, velocity, and tips of the impactor. To facilitate the prediction of the frequency response, the dynamic behavior of the resonant plate and the frequency response were estimated through finite element analysis (FEA). The predicted frequency response findings were compared with experimental results to validate the accuracy of the predictions.

The first phase of this study involves developing an impact model to analyze the force profile generated during the impact. Parameters such as hammer speed, hammer mass, hammer tip, and impacting location will be investigated to understand their effect on the force profile. This analysis aims to provide insights into the mechanics of the impact and its correlation with the subsequent pyroshock response.

In the subsequent phase, the generated force profiles from the impact model will be utilized as concentrated transient loads in a preliminary Finite Element Analysis (FEA) model of the resonant plate. Force measurement tests will be conducted to determine the actual force profile generated during the impact. The obtained force data will be compared with the results calculated from the analysis performed in SOLIDWORKS. This comparison aims to evaluate the reliability of the FEA model in capturing the impact dynamics and understanding the effect of critical test parameters.

The experimental results and comparative analysis will contribute to the comprehensive understanding of the pyroshock phenomenon and its relationship with resonant plate excitation. By validating the FEA model against actual force measurements, this research aims to enhance the accuracy and reliability of prediction models for pyroshock scenarios.

Acknowledgements

I have always been interested in the field of vibration dynamic. I have learned the course of vibration mechanics which is profoundly impacted me and make me deathly understanding and correct the vibration knowledge. Therefore, I am truly interested in and willing to explore and study the topic of pyroshock for this thesis. On another hand, the research project of pyroshock can allow me to apply the knowledge and software I have learned in the Vibration Mechanics course, which is that bring me great funny.

I would like to express my sincere gratitude to Prof. Daga Alessandro Paolo and Doc. Viale Luca for their invaluable guidance and unwavering support throughout the process of writing my thesis. when I meet any difficulties and troubles or have any questions in the research aspect, they always being patient in answering my questions and solving my difficulties and they office doors are always open to help and assist me.

CONTENT

1. Introduction

Pyrotechnic devices are specialized devices that use self-contained energy sources, such as explosives and/or pyrotechnic compositions, to release energy in the form of heat, light, gas, or sound in a controlled manner. In aerospace and defense applications, pyrotechnic devices play a crucial role in initiating critical events during space missions, such as the separation of rocket stages, deployment of satellite components, activation of propulsion systems, and various other operations that require precise timing and controlled energy release [2]. Overall, pyrotechnic devices provide efficient and controlled means for various operations in aerospace, ensuring the proper functioning and sequencing of critical events during space missions.

Pyrotechnic shock, also known as pyroshock, refers to the transient oscillatory response of a structure when subjected to high-frequency, high-magnitude stress waves generated by the detonation of pyrotechnic devices integrated into or attached to the structure [1]. However, they are significantly different compared to common mechanical shock:
1. Characteristics: Pyroshock is characterized by high peak acceleration, high-frequency content, and short duration. It is generated by the detonation of pyrotechnic devices and is highly dependent on factors such as source type, size or strength, distance from the source, and structural response. On the other hand, mechanical shock refers to the sudden impact or vibration that a structure experiences due to external forces, such as impacts, vibrations, or sudden changes in acceleration or velocity [5].
2. Frequency Range: Pyroshock typically falls within a frequency range of 100 Hz to 1,000,000 Hz, while mechanical shock can occur over a wider frequency range depending on the source and nature of the shock [5].
3. Response Behavior: Pyroshock induces an oscillatory response or ringing in the structure, characterized by multiple cycles of vibration. Mechanical shock, depending on its nature, can result in transient response or continuous vibrations.
4. Mitigation and Testing: Mitigating the effects of pyroshock often involves the use of specialized design techniques, materials, and isolation systems to protect sensitive components. Testing and characterization of pyroshock typically involve experimental and numerical simulation methods. Mechanical shock testing and analysis focus on evaluating structural integrity, dynamic response, and durability under various loading conditions.

Pyroshock typically does not cause significant damage to structural members but can result in failures in electronic and optical components that are sensitive to high-frequency energy. It can lead to relay and switch chatter, cracking or breakage of sensitive components, solder ball loosening, and deformation of lightweight structural elements. Currently, both experimental testing and numerical simulation methods are extensively employed for predicting and verifying pyroshock effects [4].

1.1 Objectives of Research

Researchers currently face a challenge due to the lack of reliable tools for accurately analyzing the generation and propagation of shock waves. Additionally, estimating and predicting the response at different locations on a structure induced by a pyrotechnic device across the entire Shock Response Spectrum (SRS) frequency range remains a significant hurdle. Therefore, it is advantageous to employ a combination of experimental and numerical simulations to address these limitations and enhance our understanding of pyroshock effects.

In this thesis research, a hammer impacting shock experiment will be employed as it offers a safe approach to generate simulated pyroshock in the laboratory. The development of a specialized algorithm capable of estimating Frequency Response Functions (FRFs) for impact tests on a resonant plate based on experimental data is currently underway. Additionally, the acceleration of many points of the plate was also recorded during the shock event, a MATLAB routine for estimating transfer functions was finally used to calculate the frequency domain response to the pyroshock in terms of inertance.

1.2 Research Methodology

The first step of this thesis involves developing an impact model to analyze the force profile generated during the impact. The study will investigate the impact of parameters such as hammer speed, hammer mass, hammer tip and impacting location on the force profile [6].

The next step of this thesis involves utilizing the force profiles generated from the impact model as concentrated transient loads in the preliminary resonant plate Finite Element Analysis (FEA) model. Force measurement tests will then be conducted to determine the actual force profile generated during the impact.

Additionally, these results from lab test will be compared with the results calculated from the analysis of SOLIDWORKS. A comparison will be made between the Finite Element Method (FEM) model's analysis predictions and the actual force measurement tests for the same configuration. This comparison aims to assess the reliability of the FEM model in comprehending the impact of critical test parameters.

2. Mechanical Impulse Pyroshock Simulator

In this report, pyroshock was simulated through a hammer impact device. To predict the impact force time history and the shock response spectrum.
For this purpose, a force measurement test setup was established, and various impact scenarios were discussed. Then, pyroshock tests by mechanical impact method were examined, performed of various configurations in the hammer [5].

In the thesis, an impact model will be created to observe the force profile formed during the impact process. Hence, the effect of four parameters such as hammer speed, additional weight, hammer tip material and impact location will be observed.
These profiles will be used as a concentrated transient load in the preliminary resonant plate model. Force measurement tests will be performed. These tests will result in the actual force profile generated during the impact.
The effects of important test parameters will also be measured by experimental setup, and these results will be compared with the results calculated from the analysis.
High level of force is generated during the impact of the hammer in the form of half sine, since the collision takes place in a very short duration, the momentum of the object turns into a high force. According to the following **Equation (2.1), (2.2)**, we can get the force versus time diagram [3].

$$J = F * \triangle t \tag{2.1}$$

$$\triangle p = m * \triangle v = F * \triangle t \tag{2.2}$$

We can get the value of impulse and the change of momentum, and the force is obtained from different sensors.

2.1 Experimental instruments

To obtain the impact force history and SRS of the resonant plate, a small-scale pyroshock simulation device was manufactured. The following table describes the equipment needed for this experiment [6].

2.1.1 Data Acquisition System

The used Data Acquisition System was an Oro's OR38 board, whose characteristics are reported in the following table.

Table 2.1 OR38 parameters

Dynamic range	24bits/140dB
Voltage range	100mv to 40v
Phase matching	20kHz
Multiple frequencies	102.4 kS/s and 65.526 KS/s with sub-multiples

The function of the acquisition system, OR38, is to collect, process, and analyze physical signals such as sound, vibration, pressure, and others. With high-performance analog-to-digital conversion technology and advanced signal processing algorithms, OR38 can accurately acquire and analyze various physical signals and provide various analysis results and reports. In addition, OR38 supports multiple interfaces and communication protocols, enabling data exchange and integration with other devices and systems.

Figure 2.1 the data acquisition system OR38

The data acquisition system will be connected to a hammer as Track 1 while eleven accelerometers will be connected to the next physical channels. It is relevant to remember that the acquisitions of the different channels are synchronous.

2.1.2 Resonant Plate

The available resonant plate is an iron plate with a thickness of 1.2 cm and a length by width of 60 cm * 36 cm. Experiments were also carried out to properly suspend the plate with steel ropes, ensuring a proper alignment to the horizontal reference.

The impact force was applied to the in-plane (front plane) orthogonal to the resonant plate while varying the mass and impact velocity of the impactor and hammer tip material [6]. A total of 5 impact points were selected, and their respective position parameters and annotation names are shown in the figure below. In absolute coordinates from the top left corner, such points can be identified as (29.7,17.5) – i.e., the center, (39.7,17.5), (49.7,17.5), (29.7,8.5) and (39.7,8.5)

Eleven sensors were installed for out-plane (rear plane) measurement. The impact force history and accelerations were respectively measured by a force transducer and shock accelerometers. To measure the entire resonant plate, data was collected in an array of 3-5-3, and the direction of impact was along the y-axis of (almost all) the accelerometers. The rear view of the plate is shown in the **Figure 2.2** below.
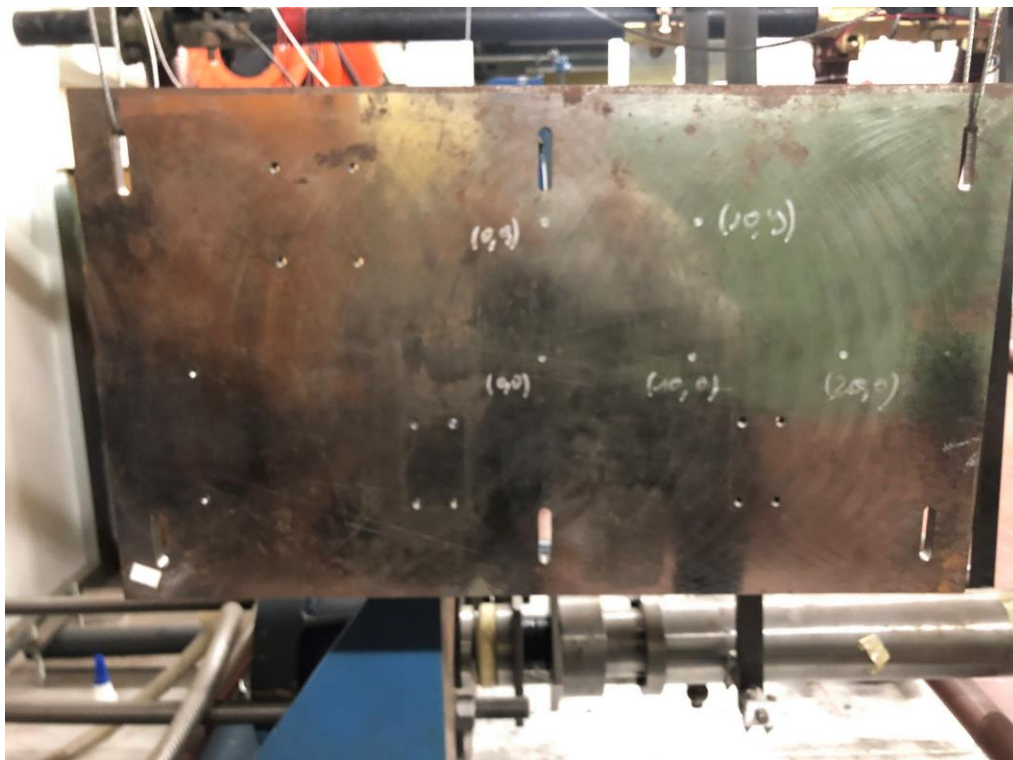
(a) front plate

(b) rear plate

Figure 2.2 front plane and rear plane in the lab
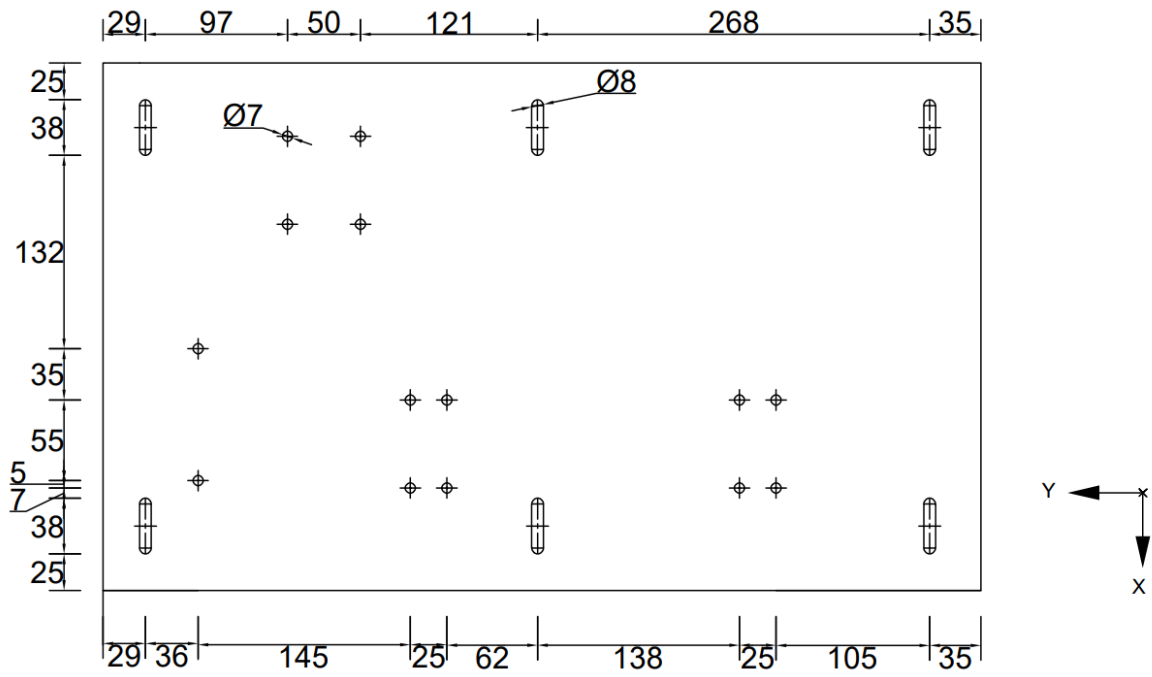
(a) front plate
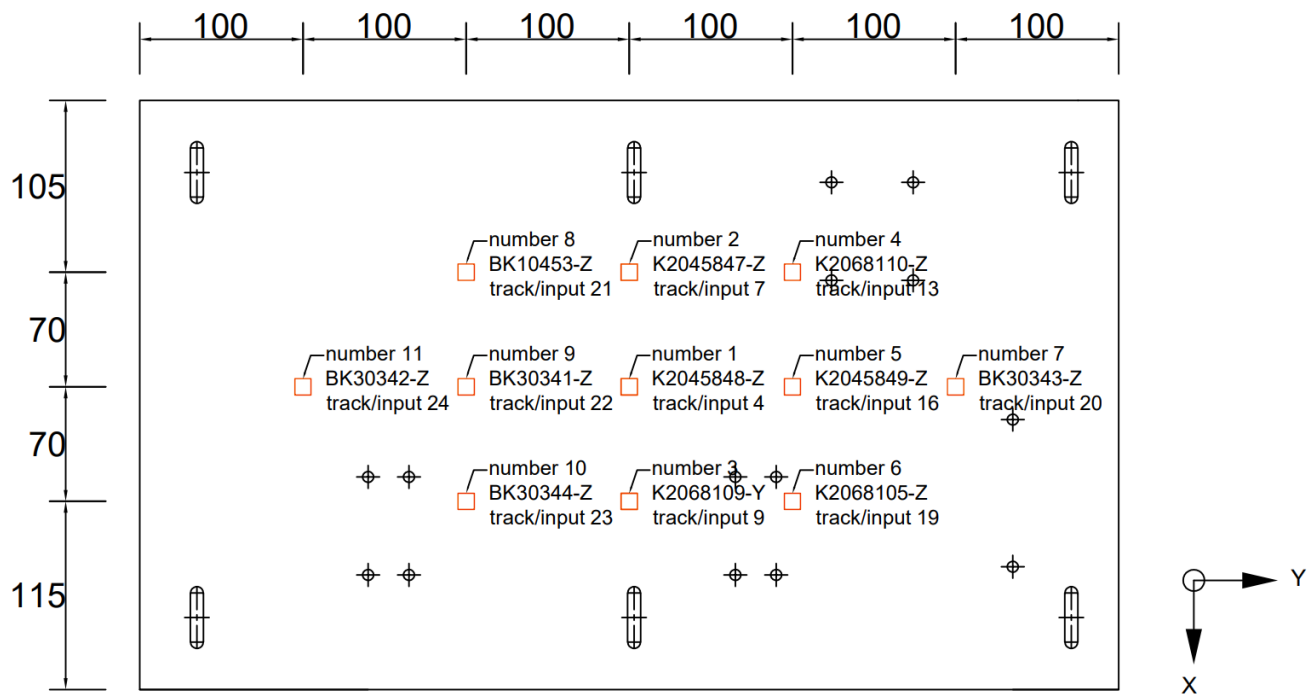
(b) rear plate

Figure 2.3 front and rear plate in the simulation

2.1.3 Sensors

In the **Table 2.2**, the primary function of an accelerometer is to measure acceleration in mechanical systems. We are using a total of 11 sensors, where 6 of them can measure all three directional axes, x, y, and z, while the remaining 5 sensors are monoaxial and measure only the Z-axis that the arrow indicates the direction of positive accelerations. The name and characteristics of all the used accelerometers are reported in the table below.

Table2.2 sensor parameters

number	sensor	accelerator range(g)	sensitivity (mv/ms^-2)	frequency range(Hz)
1	K 2045848	±500	10	12000
2	K 2045847	±500	10	12000
3	K 2068109	±500	10	12000
4	K 2068110	±500	10	12000
5	K 2045849	±500	10	12000
6	K 2068105	±500	10	12000
7	BK acc-057/30343	±70	10	6000
8	BK acc-034/10453	±70	10	6000
9	BK acc-055/30341	±70	10	6000
10	BK acc-058/30344	±70	10	6000
11	BK acc-056/30342	±70	10	6000

We position the accelerometers on the resonant plate. We connect them using the cables and as can be seen from the photos, the cables are connected both on the accelerometer and the acquisition board sides.

The eleven accelerometers are arranged in a 3-5-3 configuration to avoid the nodes of the predicted mode shapes and prevent cable bounce on the resonant plate. It is best to position the accelerometers away from the support point and the boundary to avoid generating noise and overload. Next, in the following **Table 2.3**, a detailed description of the precise locations of the accelerometers on the resonant plate is provided.

Table 2.3 Table accelerometers position on the plate and the connection port between sensors and data acquisition systems

sensor number	name	input/channel	track	direction	absolute direction	location on the plate(mm)	acquired to system
	hammer transduction	1	1				
	K 2045848	2	2	X	X	(30,17.5)	
		3	3	Y	Y	(30,17.5)	
1		4*	4	Z	Z	(30,17.5)	✔
	K 2045847	5	5	X	X	(30,8.5)	
		6	6	Y	Y	(30,8.5)	
2		7*	7	Z	Z	(30,8.5)	✔
	K 2068109	8	8	X	X	(30,27)	
		9*	9	Y	.-Z	(30,27)	✔
3		10	10	Z	Y	(30,27)	
	K 2068110	11	11	X	X	(40,8.5)	
		12	12	Y	Y	(40,8.5)	
4		13*	13	Z	Z	(40,8.5)	✔
	K 2045849	14	14	X	X	(40,17.5)	
		15	15	Y	Y	(40,17.5)	
5		16*	16	Z	Z	(40,17.5)	✔
	K 2068105	17	17	X	X	(40,27)	
		18	18	Y	Y	(40,27)	
6		19*	19	Z	Z	(40,27)	✔
7	BK acc-057/30343	20*	20	Z	Z	(50,17.5)	✔
8	BK acc-034/10453	21*	21	Z	Z	(20,8.5)	✔
9	BK acc-055/30341	22*	22	Z	Z	(20,17.5)	✔
10	BK acc-058/30344	23*	23	Z	Z	(20,27)	✔
11	BK acc-056/30342	24*	24	Z	Z	(10,17.5)	✔

2.1.4 Drop Hammer and Force Transducer Assembly

In the **Figure 2.4**, This is an assembly consisting of a drop hammer and a force transducer. We will modify this assembly by changing its mass and hammer tip to achieve our desired experimental setup. The precise description of all the used parts can be found hereinafter.

Figure 2.4 Drop hammer and force transduce assembly.

2.2 Measurement Parameters

2.2.1 Hammer Speed

The impact velocity is a continuously variable parameter. The impact velocity is controlled by the angle of bending of the arm, and the initial velocity is 0 with a fixed impact acceleration. Different speeds were tested even if a precise measurement was not possible, so the parameter was left to the sensitivity of the tester (myself).

2.2.2 Additional Weight

Looking at the **Figure 2.5**, The hammer has an initial mass which is the minimum mass it has without any add masses. There are two metal blocks available for selection: an aluminum block weighing 28 grams and an iron block weighing 80 grams. They will be installed at the tail end of the hammer.

Figure 2.5 The red marking indicates an additional weight block added.

2.2.3 Hammer Tip Material

Looking at the **Figure 2.6,2.7.2.8**, The hammerheads were manufactured in three different materials respectively, rubber tip, flat tip, and round tip. We can obtain their parameters following below **Table 2.4.**

Table 2.4 parameters of three kinds of hammer tip material

Name	Weight(g)	Material	Diameter(cm)
Rubber tip	5	Rubber	3.7
Flat tip	10	steel	3.1
Round tip	65	steel	2.3

Figure 2.6 the rubber tip
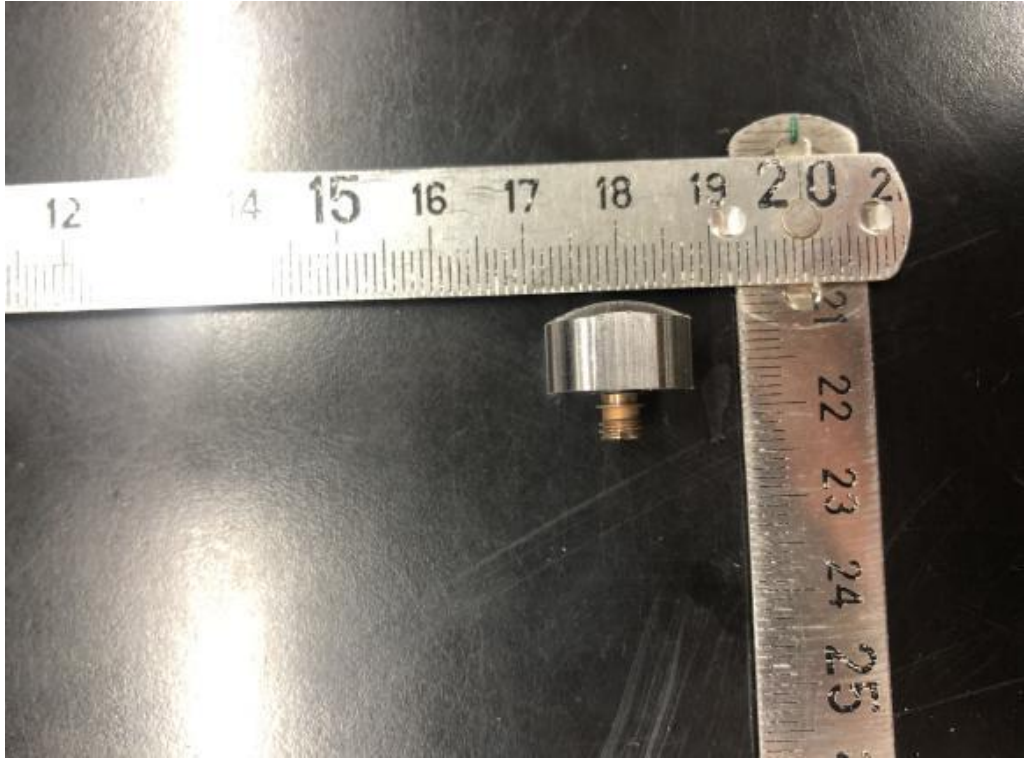
Figure 2.7 the flat tip

Figure 2.8 the round tip

2.2.4 Impacting Location

There are five different impact locations for the front plane in the **Figure 2.9**. The impact locations tested were: (29.7,17.5),(39.7,17.5),(49.7,17.5).(29.7,8.5) and (39.7,8.5). We conducted repetitive experiments by impacting each position four times. The benefits of doing so are as follows:

- Verification of the reliability and accuracy of experimental results
- Obtain optimal experimental environment: Multiple experiments can determine the best experimental environment, such as temperature, pressure, velocity, and other factors,
- Identifying abnormal results: Repetitive experiments can identify abnormal results and eliminate errors caused by operation or experimental conditions, thus obtaining more accurate experimental results.
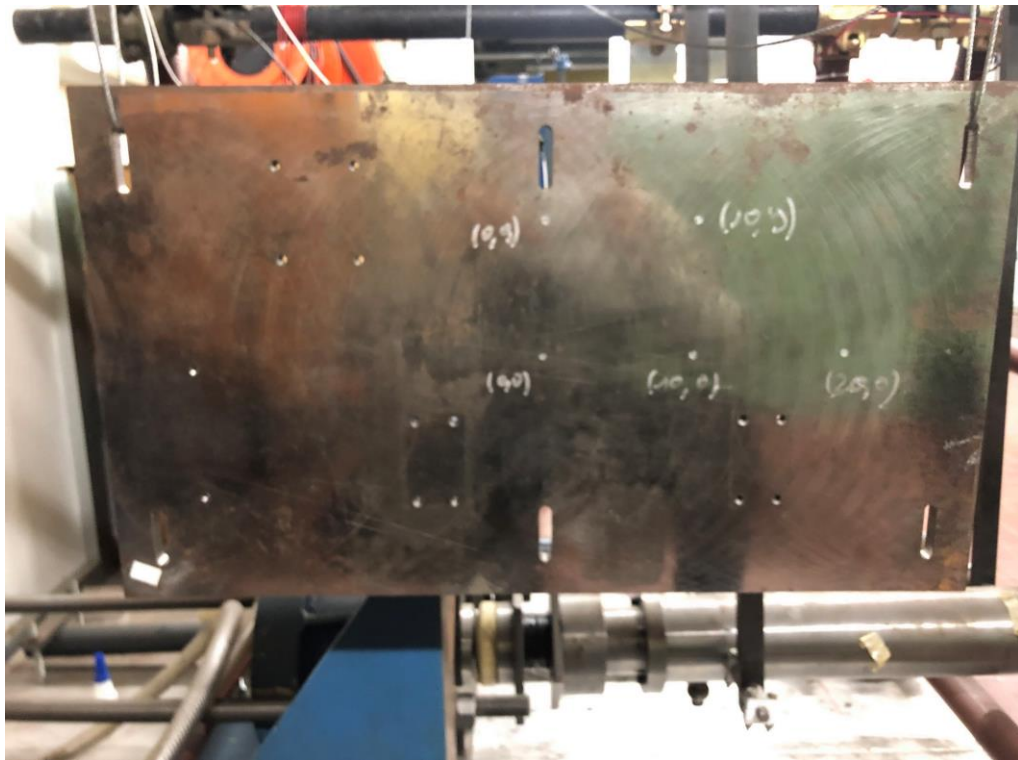
(a)lab diagram
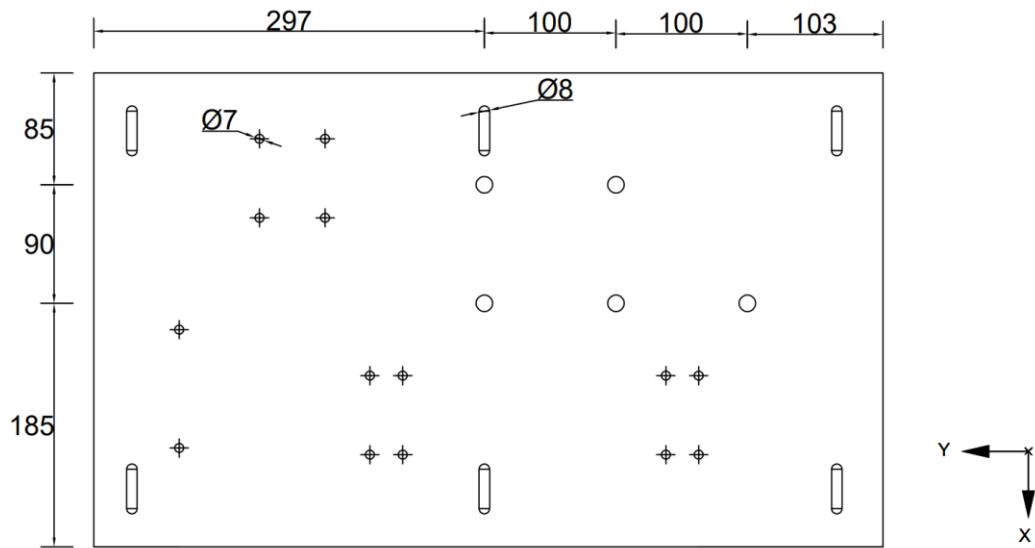
(b) simulation diagram (x axis- down, z axis -right)

Figure 2.9 five impacting locations in the plane

2.3 Force Recording from Hammer and Transducer Assembly

The small scale pyroshock simulation tests were carried out. We conducted 60 experiments with different parameters, with each impact test having four separate shocks using hammer.

We will use method of 2k factorial experiments for the design of the experiment. It is basically an experiment involving k factors, each of which has up to three levels (0,1,2). In such a multi-factor three-level experiment, the number of treatment combination needed to get complete results is equal to 2k.

Table factors have four parameters:
● A is hammer speed with low speed and high speed i.e., (0,1).
● B represents the extra weight block on the hammer, which are aluminum and Iron, respectively i.e., (0,1).
● C is hammering tips material which are rubber tip, flat metal tip and round metal tip, respectively. i.e., (0,1,2).
● D are different impacting location which have 5 locations totally. i.e.   (Center, +x, +2x, +y, +2y).

The **Table 2.5** provided below shows the recorded data from the first ten impacting tests conducted in the study (complete data can be found in the appendix). For this study, a weight of 33g, the lightest among the available options, was selected for each impact. The impacts were conducted using different combinations of conditions labeled as A,

B, C, and D.

Table 2.5. The Design of the Experiment

A: hammer speed   **(0,1 -- low speed, high speed) ,**
B : additional weight   **(0,1 -- aluminum, Ferrum)**
C: hammer tip material   **(0,1,2 -- rubber tip, flat metal tip , round metal tip)**
D: location   **(center, +x, +2x,+y, +2y)**

RUN	COMBINATION	FACTOR				weight	
		A	B	C	D		
1	.(1)	0	0	0	center (29.7,17.5)	aluminum + rubber = 33 g	
2	a	1	0	0	center (29.7,17.5)	aluminum + rubber = 33 g	
3	.(1)	0	0	0	.+x (39.7,17.5)	aluminum + rubber = 33 g	
4	a	1	0	0	.+x (39.7,17.5)	aluminum + rubber = 33 g	
5	.(1)	0	0	0	.+y (29.7,8.5)	aluminum + rubber = 33 g	
6	a	1	0	0	.+y (29.7,8.5)	aluminum + rubber = 33 g	Light
7	.(1)	0	0	0	.+xy (39.7,8.5)	aluminum + rubber = 33 g	
8	a	1	0	0	.+xy (39.7,8.5)	aluminum + rubber = 33 g	
9	.(1)	0	0	0	.+2x (49.7,17.5)	aluminum + rubber = 33 g	
10	a	1	0	0	.+2x (49.7,17.5)	aluminum + rubber = 33 g	

We will repeat 4 times for four parameters that obtain a repeatability of the results. We need to measure force and acceleration and analyze the force and we compute features that can be the area of the impact and the duration of impact that will characterize the experiment. So, every line corresponds to an experiment, involving four impacts; from each we'll have a force area, impact aera and time duration, which are the selected characteristics of the impact force.

After conducting 60 impacting tests, we have filled the following table. **Table 2.6** below shows only the results of the first ten tests, while a complete analysis of all tests is provided in Appendix 2.
- "Number" represents the experiment number, and we have a total of 60 impacting tests.
- "Impact number" represents the number of impacts for the same location under identical conditions.

- "Fmax" represents the maximum applied force.
- "Tmax" represents the duration of the applied force.
- "Δt" represents the time difference of the half-sine response.
- "Δt_left" represents the left time difference of the half-sine response.
- "Left area" represents the area on the left side of the peak force value, which represents the impulse.
- "Right area" represents the area on the right side of the peak force value, which represents the impulse.
- "Totally area" represents the total area of the impulse on the side of the peak.
- "Restitution coefficient" represents the percentage of the right area compared to the total area.

Table 2.6 The data for the first ten force measurements

number	Impact number	Fmax(N)	Tmax(S)	Δt(s)	Δt_left(s)	left area (N*s)	right area (N*s)	totally area (N*s)	restitution coefficient
t1	t1-1	235.8161	2.3540	4.9805E-04	2.5391E-04	0.0347	0.0345	0.0693	0.4985
	t1-2	279.3109	4.3977	4.8828E-04	1.9531E-04	0.0385	0.0439	0.0824	0.5326
	t1-3	375.8254	6.6607	4.6875E-04	2.3438E-04	0.0512	0.0554	0.1066	0.5199
	t1-4	442.0471	9.1890	4.7852E-04	2.5391E-04	0.0619	0.0634	0.1253	0.5058
t2	t2-1	670.7101	2.5539	3.9063E-04	1.8555E-04	0.0810	0.0935	0.1745	0.5360
	t2-2	585.5712	4.7296	4.6875E-04	2.0508E-04	0.0780	0.0810	0.1590	0.5093
	t2-3	646.2350	6.7853	4.6875E-04	2.0508E-04	0.0855	0.0910	0.1765	0.5155
	t2-4	753.3681	9.0696	4.7852E-04	2.1484E-04	0.0976	0.1040	0.2016	0.5158
t3	t3-1	315.4279	2.0539	4.7852E-04	2.0508E-04	0.0402	0.0463	0.0866	0.5353
	t3-2	365.5366	4.0229	4.6875E-04	1.8555E-04	0.0450	0.0554	0.1004	0.5520
	t3-3	492.9067	5.9781	3.9063E-04	1.7578E-04	0.0614	0.0661	0.1275	0.5182
	t3-4	502.8966	7.9813	2.9297E-04	2.3438E-04	0.0634	0.0283	0.0917	0.3084
t4	t4-1	597.8787	2.4755	4.7852E-04	2.1484E-04	0.0776	0.0824	0.1600	0.5153
	t4-2	640.7916	4.3617	4.7852E-04	1.9531E-04	0.0779	0.0945	0.1724	0.5482
	t4-3	638.7474	6.2336	4.7852E-04	2.0508E-04	0.0826	0.0880	0.1707	0.5157
	t4-4	867.2153	8.1578	3.9063E-04	1.7578E-04	0.1032	0.1140	0.2171	0.5249
t5	t5-1	403.4285	2.0210	3.9063E-04	1.7578E-04	0.0490	0.0582	0.1072	0.5429

t5-2	404.3913	3.7672	4.5898E-04	1.8555E-04	0.0504	0.0597	0.1100	0.5423
t5-3	409.4936	5.7940	4.7852E-04	1.9531E-04	0.0521	0.0588	0.1109	0.5299
t5-4	520.7382	7.6224	4.7852E-04	1.9531E-04	0.0614	0.0749	0.1363	0.5496

We conducted force measurement tests using three different hammer tips material to investigate the impact force profile's sensitivity.

Then we categorized and analyzed the experimental results into six groups **Table 2.7** based on the hammer tip material and weight, which are:

Table 2.7. weight of six different cases

1.	aluminum + rubber = 33g
2.	iron + rubber = 85g
3.	aluminum + flat = 38g
4.	iron + flat = 90g
5.	round = 65g
6.	iron + round = 93g
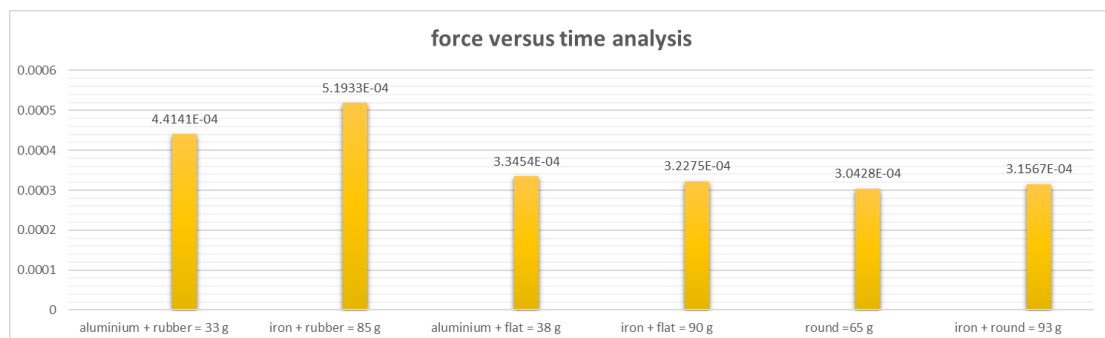
Figure 2.10 The six groups of experiments were compared based on the impulse duration.

Looking at **Figure 2.10**, these all data is measured from all Z direction of eleven sensors on the rear plate. The six data groups have the same impacting velocity, tips, and location. The only differing factor is the weight. Therefore, we divided the six groups into two categories based on weight the lightweight category consisting of the first, third, and fifth groups, and the heavy weight category consisting of the second, fourth, and sixth groups:

Category	Weight (g)	The time duration of impulse (s)
Light	Aluminium+rubber=33g	4.4141×10^{-4}
	Aluminium+falt=38g	3.3454×10^{-4}

	Round =65g	3.0428×10^{-4}
Heavy	Iron+rubber=85g	5.1933×10^{-4}
	Iron+flat = 90g	3.2275×10^{-4}
	Iron+round=93g	3.1567×10^{-4}

From these two categorized data sets, we can observe a tendency: as the weight increases, the response time decreases. Obviously, the response time ranges from 4.41×10^{-4}(33g) to 3.04×10^{-4}(65g)in the lightweight category, and from 5.19×10^{-4}(85g) to 3.15×10^{-4}(93g) in the heavy weight category.

According to **the Formula 2.1**, we can get the formula which is that frequency and the reciprocal of time difference are directly proportional. A shorter time difference in a sine signal indicates a higher frequency. Therefore, the iron plus round combination exhibits the highest frequency, while the iron plus rubber combination demonstrates the opposite.

2.3.1 Force Recording for Four Consecutive Impacts on the Same Point

We conducted a series of impact tests under the following conditions:
- A represents low velocity
- B represents the weight of the aluminum block
- C represents the rubber tip
- D represents the center point.

Four consecutive impact tests were performed, and the variations in force were recorded for each test. The obtained force values over time are as follows:
- (2.354, 235.8) represents the impulse time (2.354s) and the maximum impacting force (235.8N).
- (4.397, 279.3) represents the impulse time (4.397s) and the maximum impacting force (279.3N).
- (6.66, 375.8) represents the impulse time (6.66s) and the maximum impacting force (375.8N).
- (9.189, 442) represents the impulse time (9.189s) and the maximum impacting force (442N).

Using MATLAB's numerical processing and plotting capabilities, I analyzed the data and plotted a graph illustrating the relationship between force and time. The code can refer to the appendix A.1 'Algorithm with Force-Time Relationship at the Center Point'.

Looking at **the Figure 2.11,** The results indicated that the force gradually increased with each successive impact under these conditions and the applied impact force leads to an amplified vibration response in the tested object.
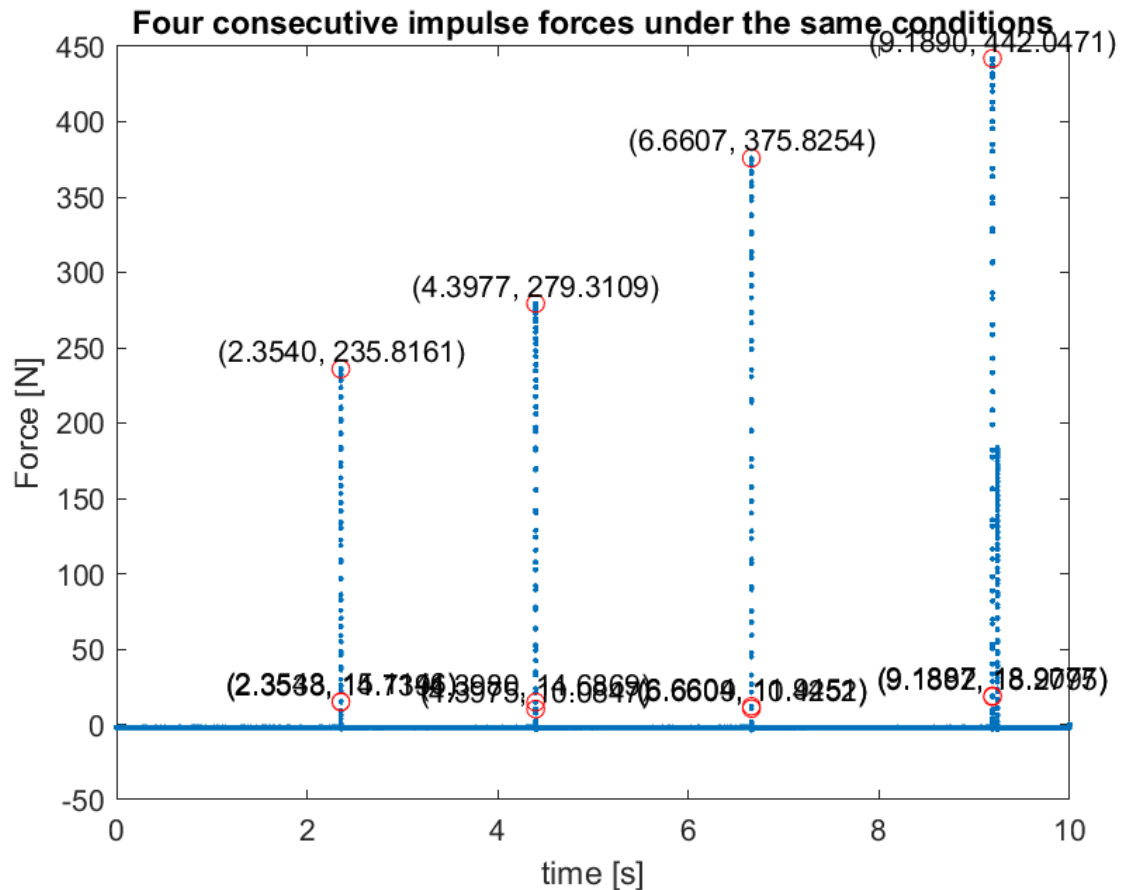
Figure 2.11 four consecutive impacting tests at the same location

2.3.2 Impulse Force Test with Hammer (Partial Segment)

Examining the **Figure 2.12**, We intend to perform data segmentation on the consecutive series of four impacts described earlier, isolating the first impact. By utilizing MATLAB code, we aim to generate the corresponding half-sine waveform under the same conditions. The code can refer to the appendix A.1- 'Algorithm with Force-Time Relationship at the Center Point'.

Next, I will explain the data presented in the graph:

- "Fmax" represents the maximum applied force.
- "tmax" represents the duration of the applied force.
- "T" represents the time difference of the half-sine response.
- "iL----Left area" represents the area on the left side of the peak force value, which represents the impulse.
- "iR----Right area" represents the area on the right side of the peak force value, which represents the impulse.
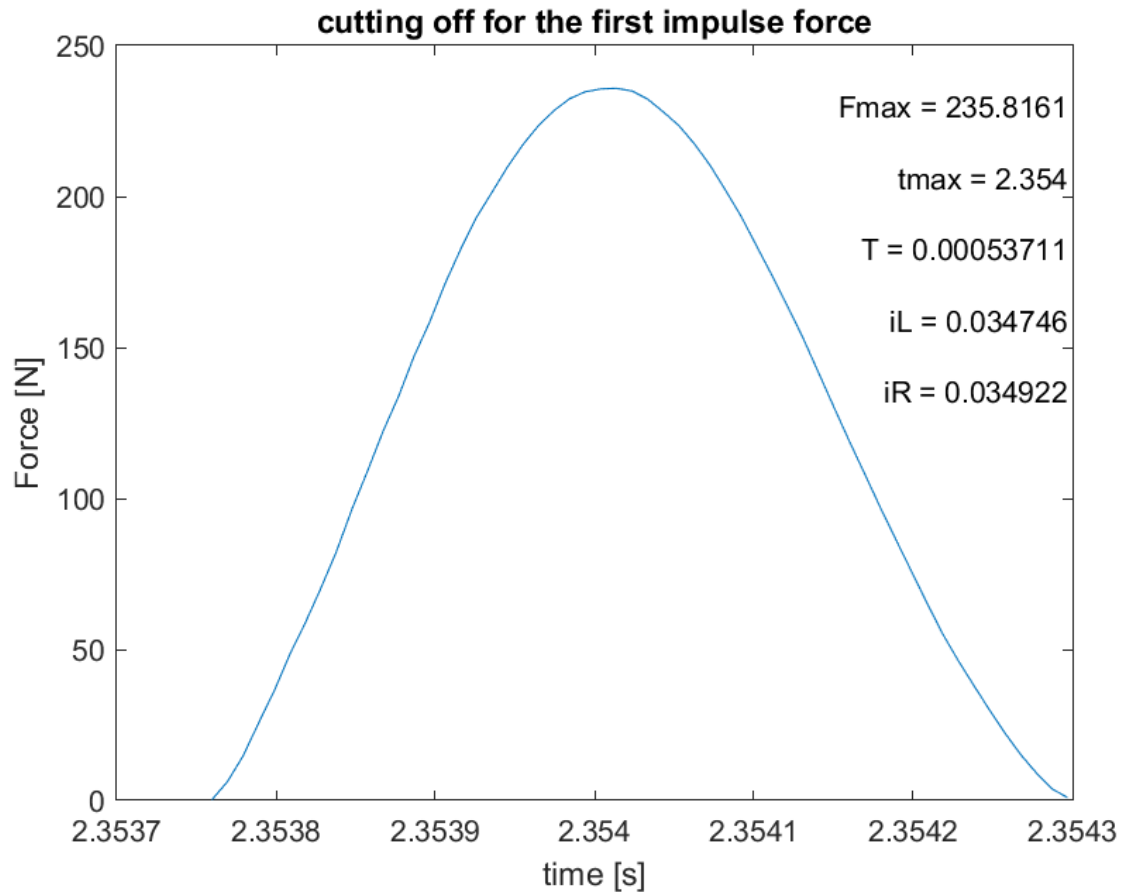
Figure 2.12 a cutting part of impacting force test with hammer

2.4 Acceleration and Frequency Recording Using Sensors

We also conducted a series of impact tests under the following conditions under the same impact conditions as before:

A represents low velocity

B represents the weight of the aluminum block

C represents the rubber tip

D represents the center point.

2.4.1 Continuous Acceleration Recording at a Fixed Point for Four Consecutive Impacts

We will utilize a total of 11 sensors to collect the acceleration data. Among these sensors, we will focus on sensor K2045848 which located on the plate ($300mm \times 175mm$) and record the acceleration values in the Z-axis direction. Using MATLAB code, which is the appendix A.2- 'Algorithm with Acceleration-Time Relationship at the Center Point'. For detailed parameters, please refer to the

Table 2.8.

Looking at the signal in **Figure 2.12**, we can generate a graph depicting the relationship between force and time, as well as compare it with the graph illustrating the acceleration over time. The force profile is represented by a solid blue line, while the acceleration profile is represented by a dashed black line. Interestingly, we observe that the amplitudes of the two profiles are nearly identical, and they both increase as the force increases.

Table 2.8 recoding of acceleration for sensor K2045858

number	impact number	Amax(m/s^2)	Tmax(S) total 10 seconds	Δt(s)	Δt_left(s)	left area(N*s)	right area(N*s)	totally area(N*s)	restitution coefficient
	t1-1	9.11239	2.35396	2.35396	8.78906E-05	2.41766E-04	2.24534E-04	4.66300E-04	4.81523E-01
t1_track4	t1-2	4.78076	4.4063	4.4063	8.78906E-05	1.56511E-04	1.31218E-04	2.87729E-04	4.56046E-01
	t1-3	12.12577	6.66063	6.66063	8.78906E-05	3.63324E-04	3.52000E-04	7.15324E-04	4.92084E-01
	t1-4	12.46871	9.18896	9.18896	8.78906E-05	4.99784E-04	4.86836E-04	9.86620E-04	4.93438E-01
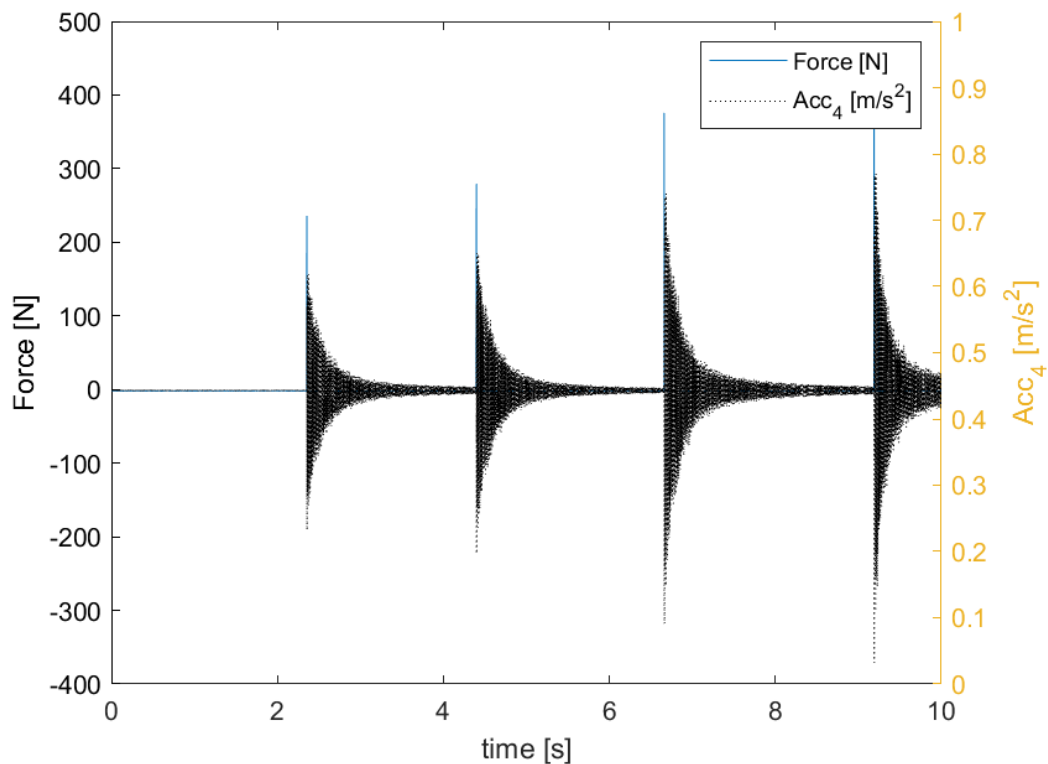
Figure 2.12 acceleration versus time for sensor K2045858

2.4.2 Impulse Force Test with Hammer (Partial Segment)

We intend to perform data segmentation on the consecutive series of four impacts described earlier, isolating the first impact. By utilizing MATLAB code, we aim to generate the corresponding half-sine waveform under the same conditions. The code can refer to the appendix A.2- 'Algorithm with Acceleration-Time Relationship at the Center Point'.
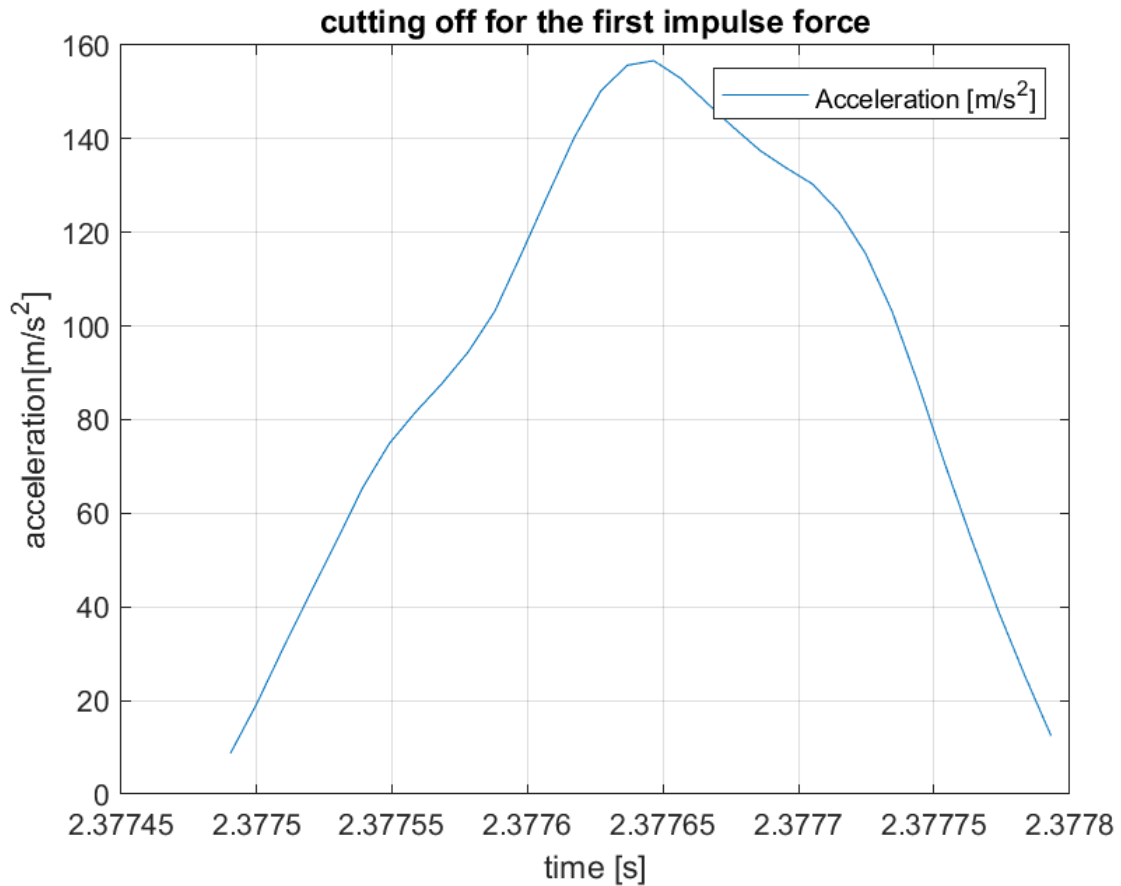
Figure 2.13 cutting off for the first impulse force

2.4.3 Fast Fourier Transform

Looking at the signal in **Figure 2.14**, as the acceleration is not constant during the test and the acceleration varies throughout the test, exhibiting a gradually decaying sinusoidal trend that approaches zero. These variations in acceleration correspond to different phenomena occurring at different times during the impact test. To better understand these phenomena, it is beneficial to separate the contributions of different harmonics. The Fast Fourier Transform (FFT) algorithm can be employed for this purpose. By applying the FFT, the original signal, which is defined in the time domain, can be analyzed in the frequency domain. This allows for easier identification and distinction of the various frequency components present in the measured signal.
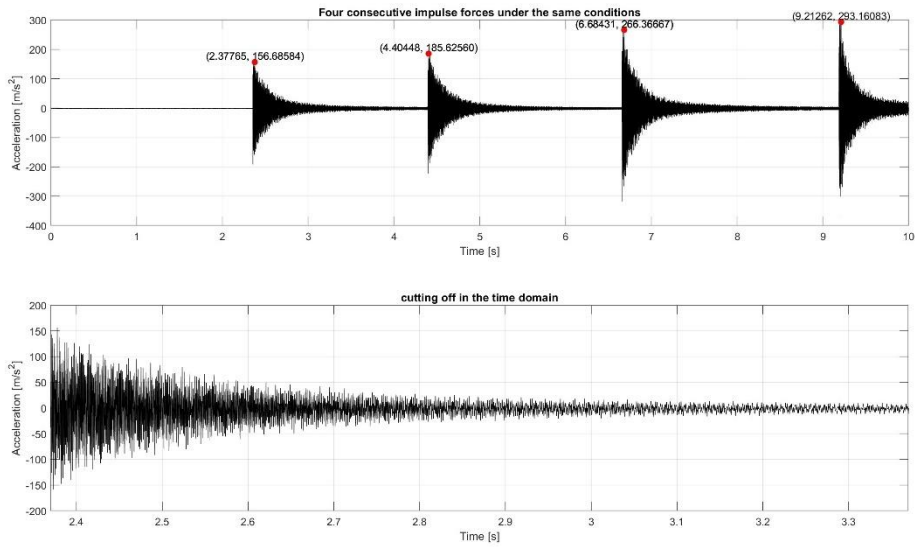
Figure 2.14. acceleration response within 10 seconds

In this study, MATLAB is employed as the environment for signal processing and analysis. Therefore, it is essential to provide a description of how the various tools are implemented in MATLAB codes. For a detailed guide on using the Fast Fourier Transform (FFT) algorithm for sensors, please refer to Appendix A.3 of this document. FFT allows for the decomposition of complex time domain signals into their constituent frequency components. After the computation of the FFT algorithm, the main information can be inferred, the amplitudes of the various contributions. By the results **Figure 2.15**, the first resonant frequency is 178.5 Hz, and the amplitude is $20.5 \ m/s^2$.
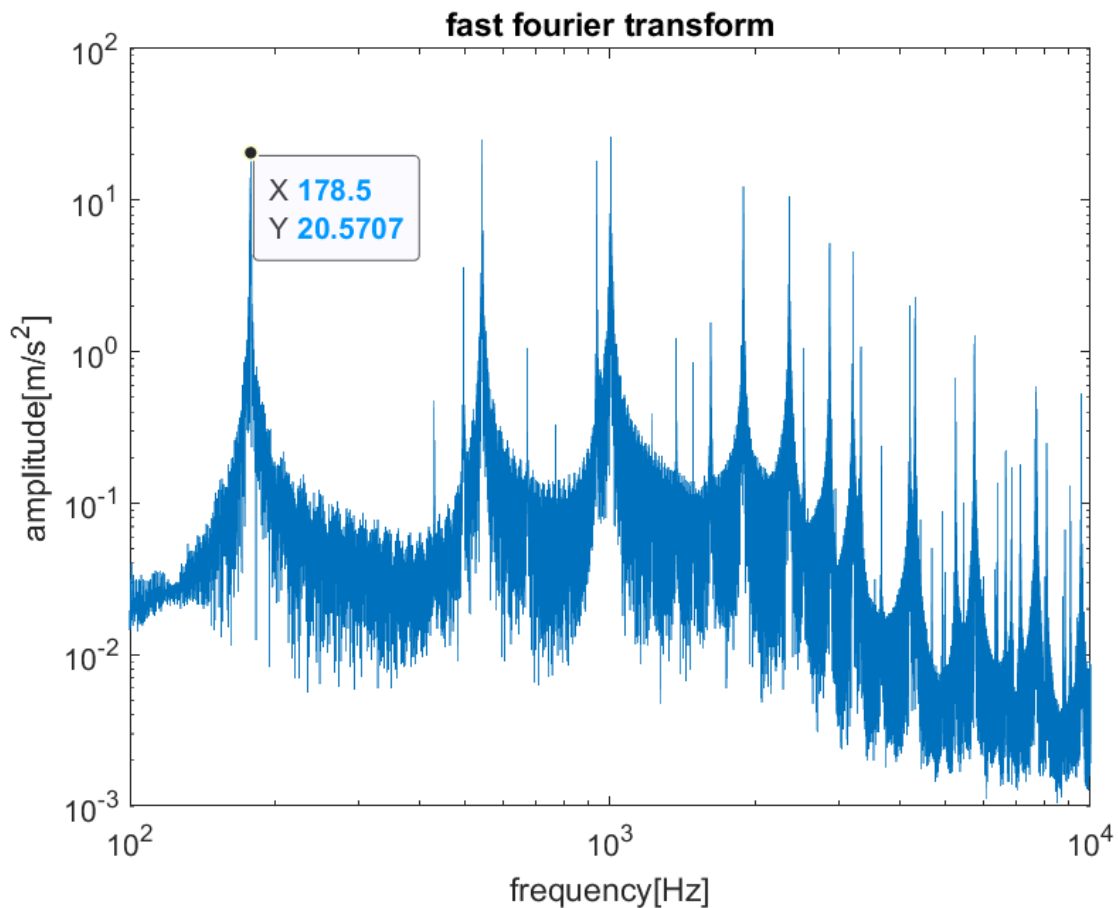
Figure 2.15 FFT for sensor Track 4

2.4.4 Transfer Function Estimation

"tfestimate" is a MATLAB function commonly used in system identification and signal processing tasks to estimate the transfer function of a signal. Its primary purpose is to determine the frequency response of a system. The function achieves this by dividing the cross-power spectrum of the input and output signals by the auto-power spectrum of the input signal [7].

In the MATLAB environment, the tfestimate function allows for the computation of the complex transfer function, enabling the extraction of magnitude and phase as a function of the excitation frequency of the resonant plate. Additionally, the function "mscohere" provides the coherence, a detailed analysis of the estimation reliability obtained through the tfestimate command, providing point-by-point insights into the estimation process.

```
N_Track1=length(Track1);              %calculates the length of the array
                                       'Track 1 '
fs=Track1_TrueBandWidth*2.56;         % calculates the sampling frequency
t=(0:length(Track1)-1)/fs;            %creates a time vector
M=floor(N_Track1/4);
```

```matlab
tfwindow= M;                         %dimension of the window
NFFT =M;                             % sampling point, set the number of
                                            the points
tfnoverlap = floor(.9*M);            % overlap of the windows

[Tf,f]=tfestimate(Track1,Track4,tfwindow,tfnoverlap,NFFT,fs);
[Tfc,fc]=mscohere(Track1,Track4,tfwindow,tfnoverlap,NFFT,fs);

figure,
subplot(3,1,1)
plot(f,20*log10(abs(Tf)),'-')
set(gca,'xscale','log')
xlim([0 10000])
xlabel('frequency[Hz]')
ylabel('Mag[dB]')

subplot(3,1,2)
plot(f,angle(Tf).*180/pi,'-')
set(gca,'xscale','log')
 xlim([0 10000])
xlabel('frequency[Hz]')
ylabel('Phase[deg]')

subplot(3,1,3)
plot(fc,Tfc)
set(gca,'xscale','log')
xlim([0 10000])
xlabel('frequency[Hz]');
ylabel('coherence');
ytickformat('%.0f');
```

Algorithm 2.1 tfestimate in the MATLAB

The final outcomes of the transfer function estimation are represented by the three plots illustrated in **Figure 2.16**. These plots provide information about the magnitude, phase, and reliability of the estimated values for each frequency. By analyzing these plots, one can determine the magnitude and phase response at different frequencies, as well as assess the reliability or confidence level associated with these estimates.
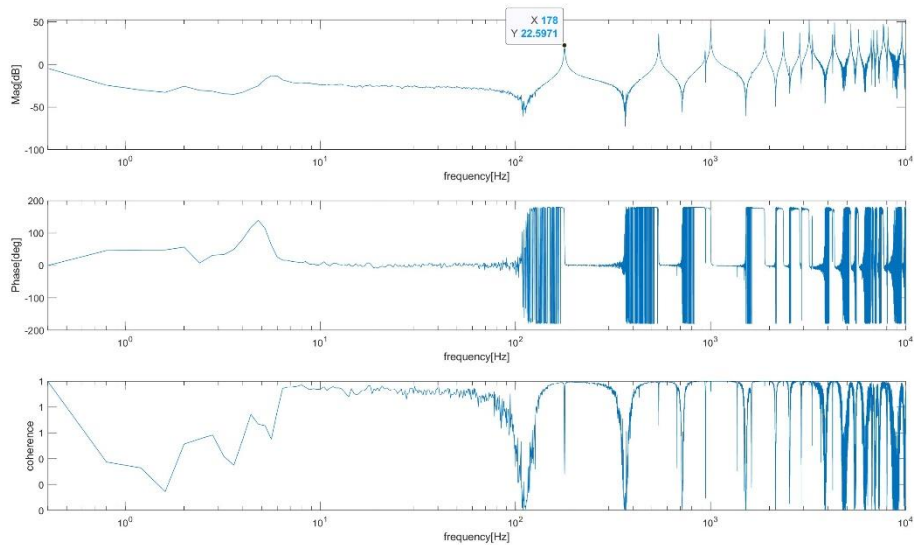
Figure 2.16 result of transfer function estimate and coherence

Upon observing the results concerning the magnitude estimation, it can be observed that the resonant plate exhibits effective vibrations attenuation in the frequency range below 100 Hz. At a frequency of 178 Hz, a resonance peak is evident, which corresponds to the characteristic resonance frequency of the resonant plate's first bending mode.

2.4.5 Prony Test – Experimental Modal Analysis

The "tfestimate" algorithm has been used to determine the frequency response and phase of a system. However, to obtain more comprehensive information for modal analysis, we introduce the "Prony test" and "FEM test" algorithms. These codes can estimate from data or from a model the resonance frequencies, the mode shapes, and modal damping, aiding in the identification of the inherent characteristics of a structure or system. They provide valuable insights into the dynamic behavior and natural modes of the analyzed system, enhancing our understanding of its modal properties.

The Prony method is a signal processing tool based on the decaying exponential model, used to estimate the vibration modes and parameters within a signal. It involves sampling the signal to obtain a discrete set of data points, forming a discrete signal sequence. The discrete signal sequence is then fitted to a sum of exponential functions model using techniques such as least squares or maximum likelihood estimation. This process allows for the calculation of the amplitude coefficients and decay rates for each exponential function. From the fitting results, parameters such as vibration mode frequencies, damping ratios, and amplitudes can be extracted.

```
f1_est=mean([f1_1,f1_2,f1_3,f1_4,f1_5,f1_6,f1_7,f1_8,f1_9,f1_10,f1_11])
d1_est=mean([d1_1,d1_2,d1_3,d1_4,d1_5,d1_6,d1_7,d1_8,d1_9,d1_10,d1_11])

A1=A1_1/A1_1;
A2=A1_2/A1_1;
A3=A1_3/A1_1;
A4=A1_4/A1_1;
A5=A1_5/A1_1;
A6=A1_6/A1_1;
A7=A1_7/A1_1;
A8=A1_8/A1_1;
A9=A1_9/A1_1;
A10=A1_10/A1_1;
A11=A1_11/A1_1;
a1=angle(A1)*180/pi
Z=[abs(A1),abs(A2),abs(A3),abs(A4),abs(A5),abs(A6),abs(A7),abs(A8),abs(A9
),abs(A10),abs(A11)];
figure;plot3(X,Y,Z,'.'),grid on
hold on;quiver3(X,Y,zeros(size(X)),zeros(size(X)),zeros(size(X)),Z,'off')
title(['Prony Estimate of First Modal Shape - f1='
num2str(floor(f1_est*100)/100) 'Hz, \zeta ='
num2str(floor(d1_est*100)/100)])
view(-5,16)
```

Algorithm 2.2 PRONY test in the MATLAB

By looking at **Figure 2.17**, we can get a three-dimensional plot where each point represents the position of a different sensor along with its corresponding data. The input signal corresponds to a force (Track 1), and the output signal is composed of acceleration from various sensors (the 11 accelerometers in the 3-5-3 arrangement). By analysis of the **Figure 2.17**, we can observe that the first modal shape is at a frequency of 178 Hz, with a damping ratio of 0.02 for the resonant plate. This shape is straightforward and clearly describes the complete behavior of a resonant plate in the first vibration mode.
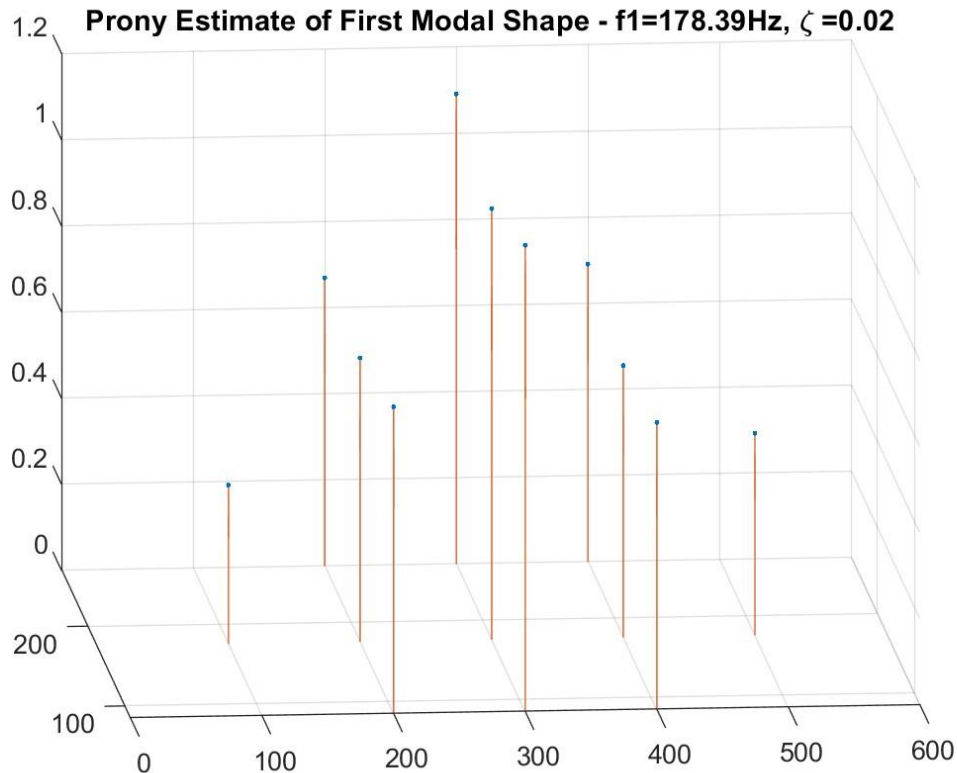
Figure 2.17 the results of Prony test

2.4.6 Finite Element Method in the MATLAB (Numerical Modal Analysis)

The modal analysis and vibration response analysis of the structure are carried out by using the finite element analysis method. It can simulate and predict the vibration response of the structure under different load conditions, and analyze the resonance frequency, modal shape, and modal mass of the structure.

In the MATLAB environment, the provided code can be explained as follows for the Finite Element Method (FEM) analysis of a resonant plate:
1. Definition of a resonant plate model, including the specification of its geometry and material properties.
2. In the modal analysis section, a structural model is created using the Partial Differential Equation (PDE) Toolbox. The model involves geometric modeling, mesh generation, setting material properties, and applying boundary conditions.
3. The 'solve' function is used to perform modal analysis on the model, calculating the natural frequencies of the resonant plate. Additionally, the mode shapes corresponding to each frequency are visualized.
4. In the frequency response analysis section, a new structural model is created, defining the geometry, mesh, material properties, and boundary conditions.

5. The 'solve' function is used again to perform frequency response analysis, computing the acceleration response at different frequencies. The resulting data is used to plot the variation of acceleration amplitude with frequency.

6. In summary, the code models and analyzes the behavior of a resonant plate structure using modal analysis and frequency response analysis. Modal analysis is used to determine the natural frequencies and mode shapes of the resonant plate, while frequency response analysis provides insights into the acceleration response of the plate at different frequencies.

The following is a partial code snippet. For more detailed information, please refer to Appendix A.6.

```matlab
%% Disc Model Definition
a=0.600;                              %m
b=0.360;                              %m
h=0.012;                              %m
r=0.005;                              %radius of contact
gm = multicuboid([r a],[r b],h);
hmax = h/2;                           %for mesh size

%MATERIAL: PLAIN STEEL
E=2.1E11;                             %Pa
v=0.3;                                %Poisson
ro=7800;                              %kg/m3

%% Analytic sol, Blevins
i=3;
j=1;
Lam2=pi^2*(GG(i)^4+(a/b)^4*GG(j)^4+2*(a/b)^2*(JJ(i)*JJ(j)+2*v*(HH(i)*HH(j)
)-JJ(i)*JJ(j))))^.5;
f=Lam2/(2*pi*a^2)*(E*h^2/(12*ro*(1-v^2)))^.5;

%% MODAL analysis settings
model = createpde("structural","modal-solid");
model.Geometry =gm;
figure(1)
subplot(1,3,1),pdegplot(model,"CellLabels","on","FaceAlpha",0.5),title('C
ells')
subplot(1,3,2),pdegplot(model,"FaceLabels","on","FaceAlpha",0.5),title('F
aces')

%MESH
msh = generateMesh(model,'Hmax',hmax);
figure(1)
```

```matlab
subplot(1,3,3),pdemesh(model),title('Mesh')

%MATERIAL (Plain Carbon Steel)
structuralProperties(model,"YoungsModulus",E, ...
                          "PoissonsRatio",v, ...
                          "MassDensity",ro);

%BC
structuralBC(model,"Face",1,"Constraint","free");

% SOLVE modal
modalresults = solve(model,'FrequencyRange',[10,300]*2*pi);
modalresults.NaturalFrequencies/(2*pi);

figure;
subplot(1,3,1)
pdeplot3D(modalresults.Mesh,'ColorMapData',modalresults.ModeShapes.uz(:,1
))
title(['Mode with Frequency ', ...
        num2str(floor(modalresults.NaturalFrequencies(1)/(2*pi))),' Hz'])
axis equal
subplot(1,3,2)
pdeplot3D(modalresults.Mesh,'ColorMapData',modalresults.ModeShapes.uz(:,2
))
title(['Mode with Frequency ', ...
        num2str(floor(modalresults.NaturalFrequencies(2)/(2*pi))),' Hz'])
axis equal
subplot(1,3,3)
pdeplot3D(modalresults.Mesh,'ColorMapData',modalresults.ModeShapes.uz(:,3
))
title(['Mode with Frequency ', ...
        num2str(floor(modalresults.NaturalFrequencies(3)/(2*pi))),' Hz'])
axis equal
```

Algorithm 2.3 code of Finite element method

Looking at **Figure 2.18**, we can make sure the frequencies of the first three modes respectively 178 Hz, 183 Hz, and 413 Hz. Comparing the first three frequency analysis methods, their first vibration frequency results were all 178 Hz and had the same vibration shape.

Mode with Frequency 178 Hz

Mode with Frequency 183 Hz

Mode with Frequency 413 Hz
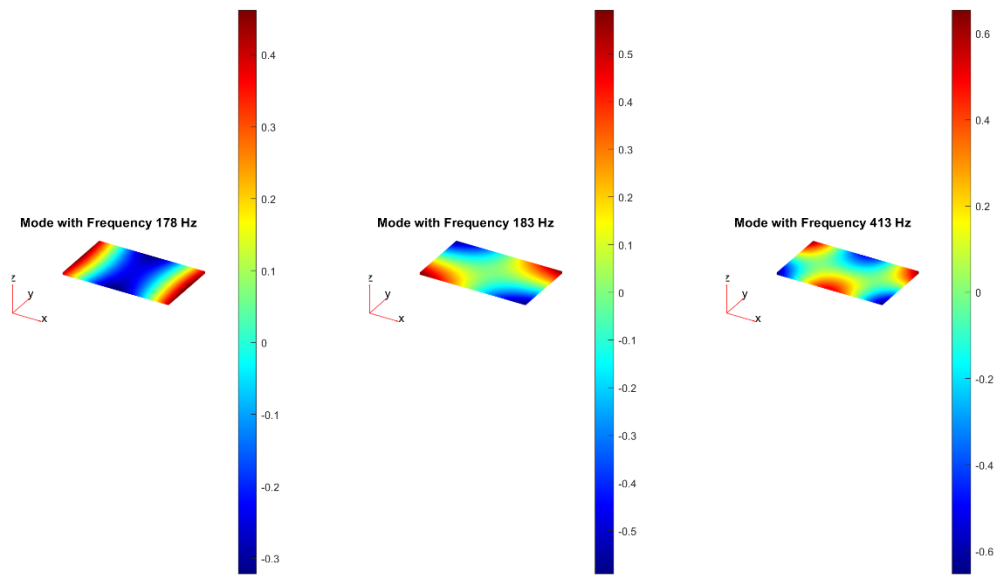
Figure 2.18 the results of FME test

3. Numerical Simulation with commercial software

The small-scale pyroshock resonant plate was designed using SOLIDWORKS, a 3-dimensional modeling program. Then the acceleration of the resonant plate was calculated by employing harmonic dynamic analysis based on the measured impact force history [6]. To validate the accuracy of the finite element analysis (FEA) model, the results of the harmonic dynamic analysis obtained through FEA were compared with the resonant frequency calculated from the pyroshock experiment. However, we also need to consider the potential error of the boundary conditions between the FEA model and the test model [4].

3.1 Model Building

Looking at the **Figures 3.1 and Figure 3.2**, we can replicate the same model using SOLIDWORKS based on the measurement data of the resonant plate from Chapter 2. In the laboratory, we conducted 60 impact experiments under different conditions and obtained output data using 11 sensors. For the simulation experiment in SOLIDWORKS, we simulated only one case where the impact was applied at the center point of the resonant plate. We placed three sensors (K2045848, K2045847, K2068110) at the back of the plate at positions $300mm \times 175mm$, $300mm \times 85mm$, and $400mm \times 175mm$ to obtain the output results.
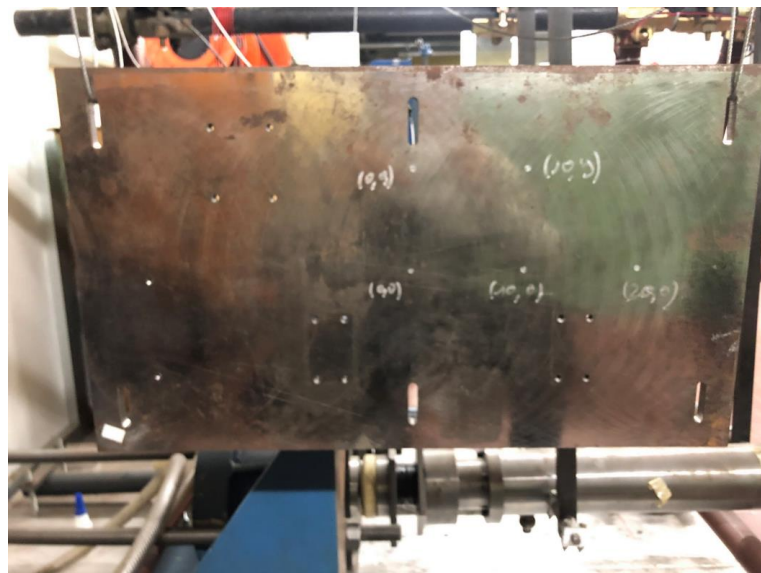
Figure 3.1 $600 \times 360 \times 12\ mm^3$ resonant plate hammer-type test system
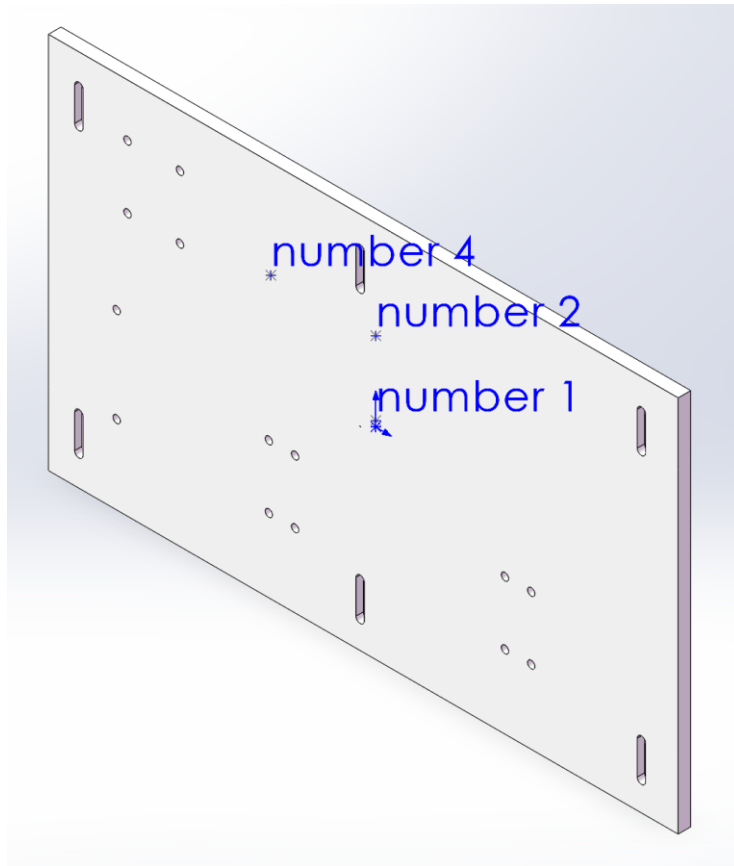
Figure 3.2 $600 \times 360 \times 12\ mm^3$ resonant plate analysis model

3.2 Frequency Simulation

Frequency analysis, also known as modal analysis, is a rapid method for predicting the vibration characteristics of the resonant plate without directly inputting the vibration source into the software. The objective is to verify that the component is sufficiently rigid to withstand potential vibration loads. Two outputs are obtained from this analysis: the mode shape of the component and its natural or resonant frequency.

The goal is to ensure that the vibration frequency does not align with the plate's resonant frequency, thereby avoiding resonance. Additionally, studying the mode shapes provides insight into how the component may vibrate.

3.2.1 Parameter Selection

Examining the **Table 3.1**, we will explore the FEA impacting parameters on the results of the analysis.

(1) In this analysis, the maximum frequency we are interested in is 10000 Hz so that runed the software to generate 100 natural frequencies. The corresponding 100-

amplitude diagram shows the different vibration mode shape of the component which is associated with a specific natural frequency.

(2) Since we do not know the material of the resonant plate, we assume it to be plain carbon steel. Its density is $7800 \ kg/m^3$, elastic modulus is $2.1 \times 10^{11} \ N/m^2$, shear modulus is $7.9 \times 10^{10} \ N/m^2$, and Poisson's ratio is 0.28.

(3) Fixing fixtures are used to completely restrict the movement and rotation of an object to keep a fixed position. Elastic supports, on the other hand, allow a range of displacements and deformations to simulate elastic behavior. In the case of simulating the experimental process, our chosen fixture is free, which means that the object is unrestricted.

(4) Finally, we choose the medium mesh density for the resonant plate. We can create a mesh mode to make it thinner or thicker, use different SOLIDWORKS'S algorithms for the geometry.

(5) Connection, which is how components interact with each other. we can skip it because we only have a complete resonant plate and nothing else that needs to be connected.

Table 3.1 parameter setting of frequency response

number of frequency	100
material	plain carbon steel
fixture	free
Mesh	medium

Looking at the **Table 3.2**, we can track the response of the system at that point using the sensor. We can observe that the resonant plate exhibits lateral vibrations in the Z direction across multiple vibration modes. The first six mode values are close to 0 Hz (corresponding to translational motion in the forward-backward and left-right (corresponding to translational motion in the forward-backward and left-right directions, as well as clockwise and counterclockwise rotations) given the free boundary conditions. From the 7th mode to the 100th mode, the natural frequencies range from 177 Hz to 10406 Hz.

Table 3.2 the mode of frequency from 1 to 100

Mode No.	Frequency(Hertz)
1	0
2	0
3	0
4	0
5	0.00018555
6	0.00066878

7	177.12
8	185.27
…..	…..
98	10294
99	10350
100	10406

3.2.1 Material Verification

Since the actual material of the resonant plate is unknown, we need to confirm our material selection based on the natural frequencies. In the laboratory, we obtained the physical parameters of the resonant plate and the resonant frequencies from the sensors. The first six resonant frequencies are 178.5 Hz, 541.8 Hz, 1002 Hz, 1894.5 Hz, 2360.5 Hz, and 2863.5 Hz.

Subsequently, we selected parameters identical to the previous ones, with the only variation being the material. We compared the first six resonant frequencies of the selected materials with the resonant frequencies of the laboratory resonant plate using the absolute value difference method.

Table 3.3 the resonant frequency and parameters of eight different materials

	cast alloy steel(Hz)	alloy steel(Hz)	carbon steel (Hz)	AISI 304(Hz)
1	174.04	243.91	181.55	173.23
2	496.12	532.78	499.99	599.15
3	974.13	1047.3	982.61	937.5
4	1823.5	1766.6	1827	1746.7
5	2347.9	2469.2	2364.2	2349.6
6	2767.4	2811.1	2750.2	2883.7
	plain carbon steel(Hz)	wrought stainless steel(Hz)	AISI 316 (Hz)	gray cast iron(Hz)
1	177.1	179.6	175.81	243.91
2	506.77	486.23	602.05	532.78
3	995.63	954.71	940.12	1047.3
4	1856.5	1787.1	1756.9	1930.1
5	2396.9	2410.1	2367.6	2396.9
6	2816.5	2946.9	2862	2811.1

	Cast alloy steel	alloy steel	carbon steel	AISI 304
elastic modulus (N/m^2)	1.90×10^{11}	2.1×10^{11}	2.05×10^{11}	1.9×10^{11}
Poisson's Ratio(N/A)	0.26	0.28	0.29	0.29
Shear Modulus(N/m^2)	7.8×10^{10}	7.9×10^{10}	8.0×10^{10}	7.5×10^{10}
mass density(kg/m^3)	7300	7700	7858	8000

	plain carbon steel	wrought stainless steel	AISI 316	gray cast iron
elastic modulus(N/m^2)	2.1×10^{11}	2×10^{11}	1.93×10^{11}	6.62×10^{10}
Poisson's Ratio(N/A)	0.28	0.26	0.27	0.27
Shear Modulus(N/m^2)	7.9×10^{10}	7.9×10^{10}		5×10^{10}
mass density(kg/m^3)	7800	8000	8000	7200

Table 3.4 the result of eight different materials using the absolute value difference method

	cast alloy steel(Hz)	alloy steel(Hz)	carbon steel (Hz)	AISI 304(Hz)
1	4.46	65.41	3.05	5.27
2	45.68	9.02	41.81	57.35
3	27.87	45.3	19.39	64.5
4	71	127.9	67.5	147.8
5	12.6	108.7	3.7	10.9
6	96.1	52.4	113.3	20.2
Sum	257.71	408.73	248.75	306.02
	plain carbon steel (Hz)	wrought stainless steel (Hz)	AISI 316 (Hz)	gray cast iron (Hz)
1	1.4	1.1	2.69	65.41
2	35.03	55.57	60.25	9.02
3	6.37	47.29	61.88	45.3
4	38	107.4	137.6	35.6
5	36.4	49.6	7.1	36.4
6	47	83.4	1.5	52.4
Sum	164.2	344.36	271.02	244.13

Analyzing the **Table 3.3 and Table 3.4**, we can observe that plain carbon steel is the closest match to our actual results. Its first resonant frequency is 177.1 Hz, which is almost identical to the first resonant frequency of the resonant plate at 178 Hz. Furthermore, compared to other materials, it has the smallest absolute value differences for the first six resonant frequencies, indicating a better alignment with the experimental data.

3.3 Harmonic Simulation

In order to get the frequency response to a force, in SOLIDWORKS it is possible to run a harmonic analysis that can be grouped under one umbrella which is the frequency-based analysis. The result will be a transfer function from force to acceleration in the frequency domain (i.e., an Inertance). This kind of frequency domain simulation was preferred to time domain simulations which are commonly heavier from a computational point of view and less stable.

Let's take harmonic analysis as an example. This analysis is used for vibrations striking a resonant plate with a hammer, where the frequency of the vibration is gradually varied to determine the amplitude for different frequency inputs. Here, instead of feeding the sinusoidal input as a function of time, we convert it to an acceleration versus frequency curve. In this way, we avoid simulating any transients and can quickly obtain acceleration output results at different loading frequencies. Another benefit of these frequency-based analyses besides saving time is that a lot of these inputs are available with design testing standards.

A harmonic dynamic analysis was run to observe the structural response and how the system behaves when forces are applied at different frequencies.

3.3.1 Parameter Selection and Result Analysis

Compared to frequency simulation, our parameter selection remains the same, but we need to introduce two new parameters: the Load and Damping ratio. To view the **Table 3.5.**
(1) We will introduce a vibration source to study the response. A uniform base excitation of 1N will be applied in the Z-direction at the center of the resonant plate.
(2) In structures, we need to include a damping ratio. If without damping in the system, there would be an occurrence of infinite resonance, which is obviously undesirable.
On the other side, it is difficult to quantify or estimate the impact of different damping sources, resulting in potential discrepancies between test measurements and simulation performance. Finally, we could choose 0.02 to try it.

Table 3.5 parameter setting of harmonic frequency

number of frequencies	50
material	plain carbon steel
fixture	free

Mesh	medium
Load	1N at the center
Damping ratio	0.02

The result **Figure 3.3** shows the deformation in the Z-direction, which is clearly exaggerated and excessive. The displacement of the column on the right can be observed, and it appears to be relatively small.
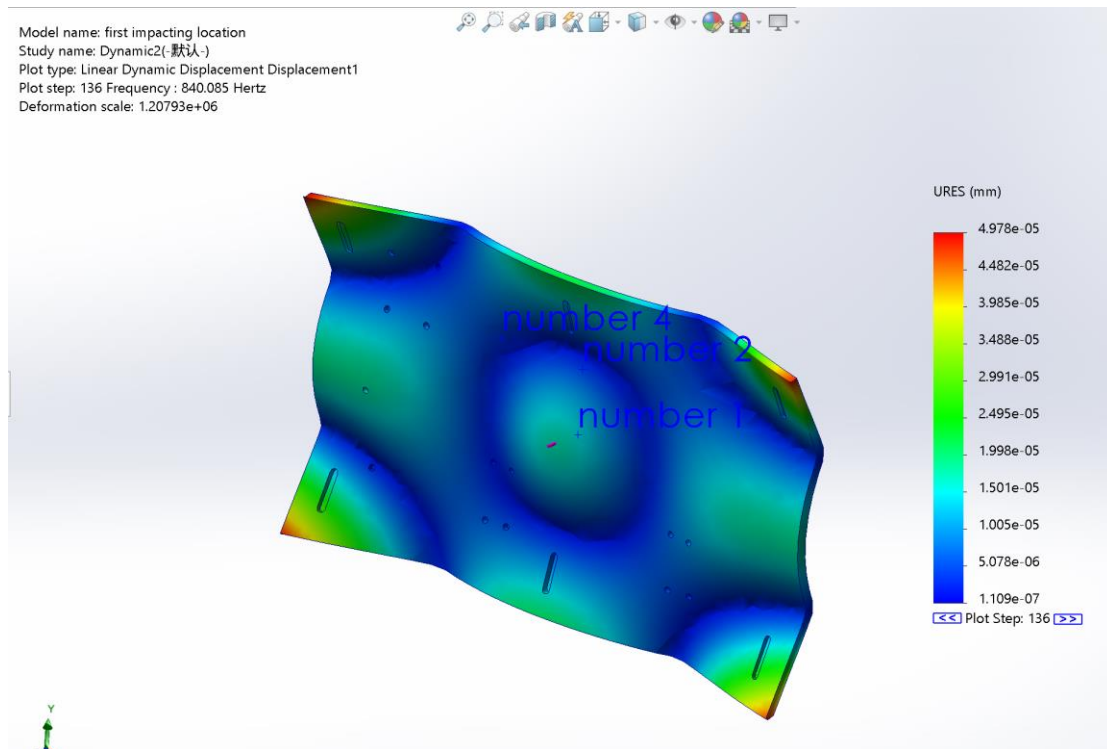
Figure 3.3 the Deformation of the plate in the SOLIDWORKS

Next, we should focus on the resonant frequencies. Looking at the response graph **Figure 3.4**, with the x-axis representing frequency and the y-axis representing acceleration, this is the desired outcome. At around 170 Hz, the first natural frequency, the amplitude is approximately $4.12 \, m/s^2$. We can then convert the graph into an Excel file for comparison with the data from the laboratory.
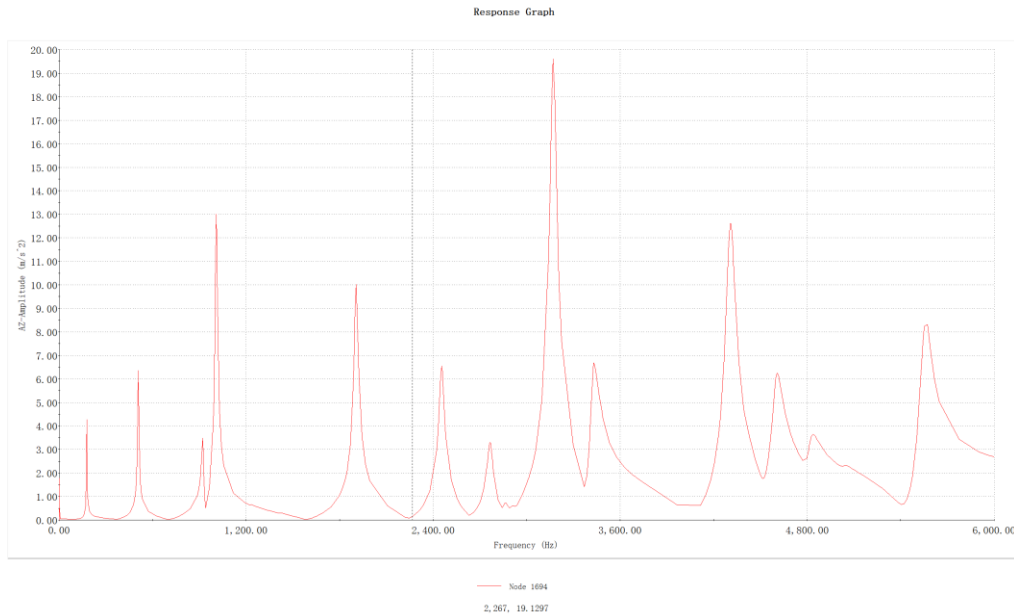
Figure 3.4 the result of harmonic test from SOLIDWORKS

Using the tfestimate algorithm in MATLAB, **Algorithm 3.1**, we obtained the resonant frequency points of the graph within the range of 10,000 Hz, **Figure 3.5**. It can be observed that the first two resonant frequencies are approximately 178 Hz and 507 Hz. This is a promising result as it closely matches the data obtained from our laboratory experiments. In the next chapter, we will comprehensively compare the simulated data with the experimental data.

```matlab
filename = 'first impacting location-0.02.csv ';        %Path and file
                                                  name of the Excel file
sheet = '1';                                       % Index or name
                                                   of the Excel sheet

range1 = 'B9:B520';                                % first area
range2 = 'C9:C520';                                %second area


data1 = readmatrix(filename,  'Range', range1);
data2 = readmatrix(filename,  'Range', range2);


figure


semilogx(data1,20*log10(abs(data2))),
xlim([1e1 1e4])
xlabel('frequency(Hz)')
ylabel('acceleration(m/s^2)')
grid on
```

Algorithm 3.1 transfer function estimate code from mode of SOLIDWORKS
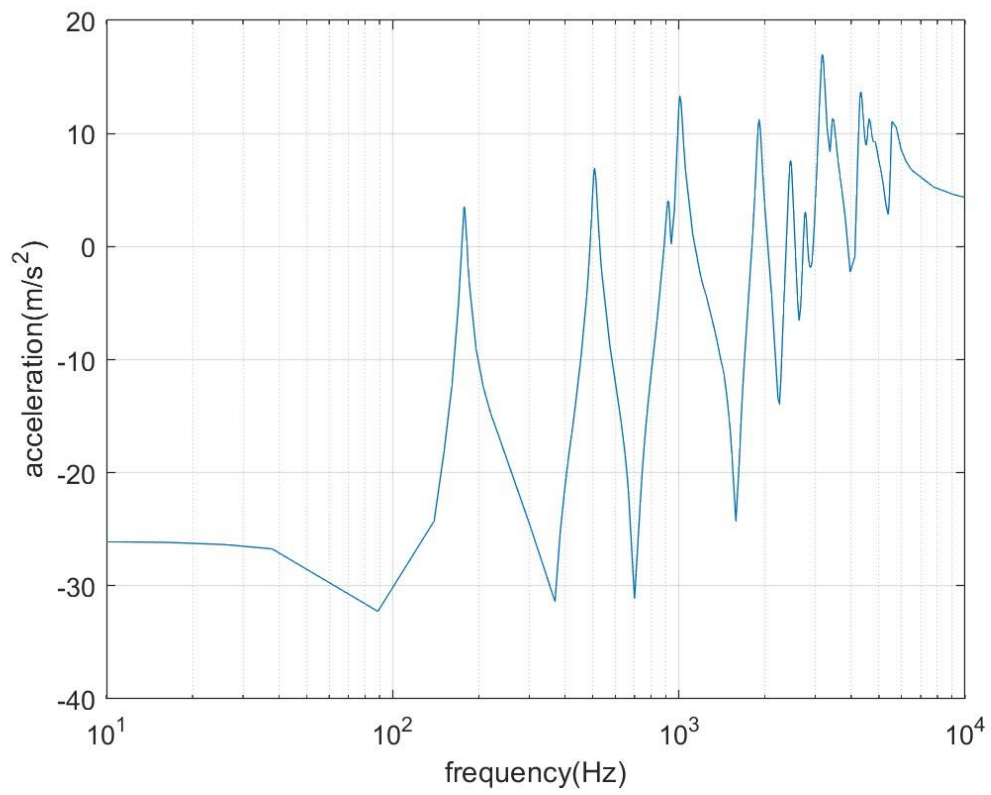
Figure 3.5 The resonant frequency of the simulation model impacted at the center point

4. Comparison of Frequency Results between Experimental Data and Numerical Simulation

This chapter presents a comparison between the analysis models and the corresponding test configurations. The analysis predictions focused on specific locations on the resonant plate, while accelerometers were strategically placed to measure out-of-plane accelerations. The transfer function estimate plots within the frequency range of 0-10,000 Hz were compared for further analysis and evaluation [5].

Looking at the **Table 4.1**, In the numerical models we have three impacting locations corresponding to the same location in the laboratory. The acceleration profiles are measured by three acceleration sensors.

Table 4.1 impacting position and sensor installation position

	Test measurement	Simulation analysis
Impacting location 1	$297mm \times 175mm$	$297mm \times 175mm$
Impacting location 2	$397mm \times 175mm$	$397mm \times 175mm$
Impacting location 3	$397mm \times 85mm$	$397mm \times 85mm$
Sensor 1	$300mm \times 175mm$	$300mm \times 175mm$
Sensor 2	$300mm \times 85mm$	$300mm \times 85mm$
Sensor 4	$400mm \times 85mm$	$400mm \times 85mm$

By MATLAB **Algorithm 4.1**, We can obtain their frequency response comparison. Upon examining **the figures 4.1,4.2,4.3** depicting the results from different impacting locations, it can be observed that the analysis predictions align well with the test results. The modal peaks exhibit similar frequencies in both the test and analysis outcomes. However, there is a notable discrepancy in the amplitude, despite the implementation of low damping coefficients at these frequencies. Therefore, further adjustments to the damping coefficients, specifically to a value of 0.001, are necessary in order to improve the accuracy of the analysis results.

```matlab
figure;
semilogx(f,20*log10(abs(Tf)),'-'), hold on
semilogx(data1,20*log10(abs(data2))),
xlim([1e1 1e4])
xlabel('frequency(Hz)')
ylabel('acceleration(m/s^2)')
title('transfer function estimate for third impacting location,damping
ratio 0.001')
```

```
legend('test measurement','analysis prediction')
```

Algorithm 4.1 comparison of frequency between experimental data and numerical simulation
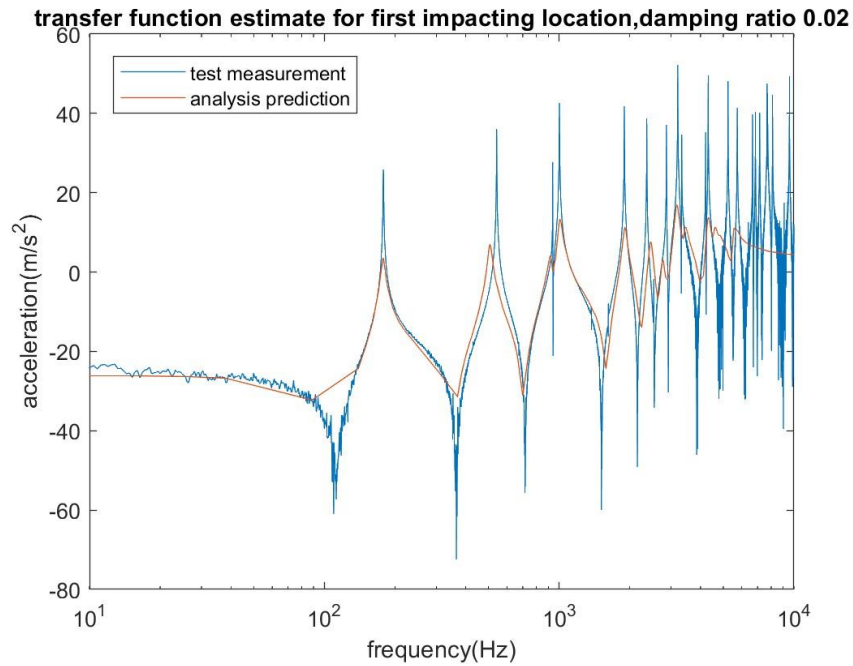
Figure 4.1 transfer function estimate for first impacting location, damping ratio 0.02
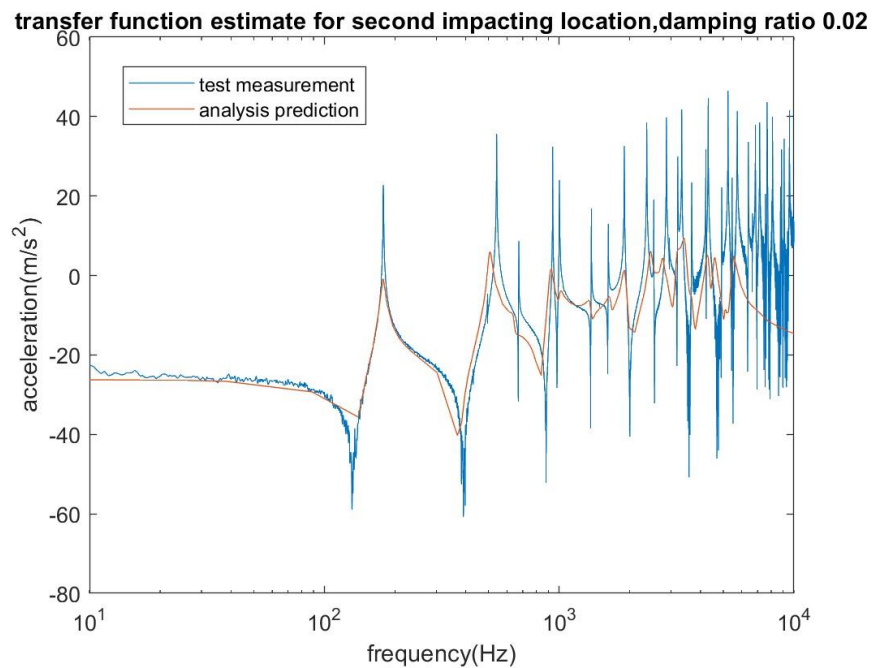
Figure 4.2 transfer function estimate for second impacting location, damping ratio 0.02
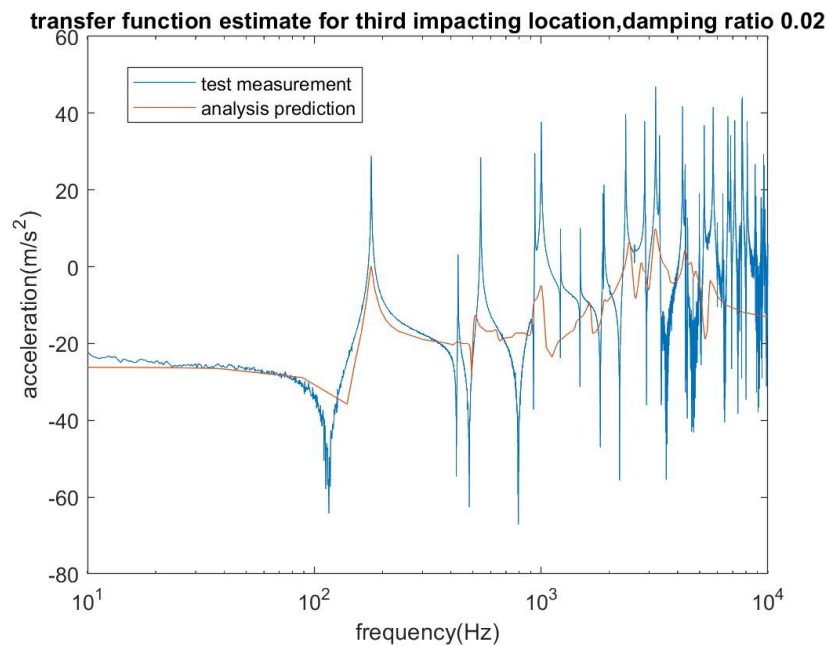
Figure 4.3 transfer function estimate for third impacting location, damping ratio 0.02

Looking at **the Figure 4.4,4.5,4.6**, the thin and long plate with dimensions of 600x360x12 mm^3 exhibited a good agreement between the analysis and experimental results after adjustments, The modal peaks were successfully matched. However, the experimental results remained slightly higher than the analysis predictions after 550 Hz. Overall, the selection of appropriate mechanical properties and finite element parameters played a significant role in achieving low error rates in the comparisons. In terms of the transfer function estimate of modal peaks, it was challenging to obtain similar matches without optimizing the modal damping ratios. However, by optimizing the modal damping ratios, almost identical results were obtained between the experiment measurements and analysis predictions.
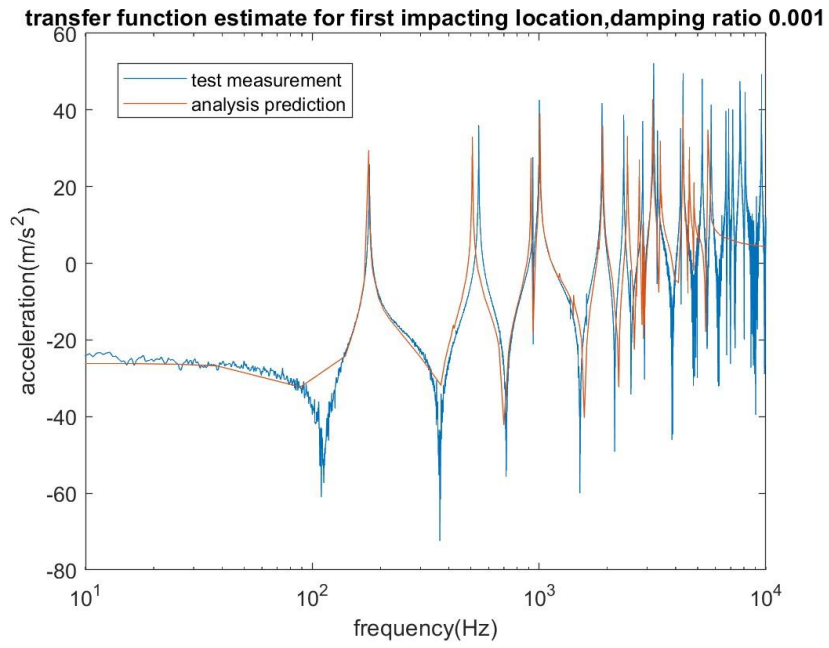
Figure 4.4 transfer function estimate for first impacting location, damping ratio 0.001
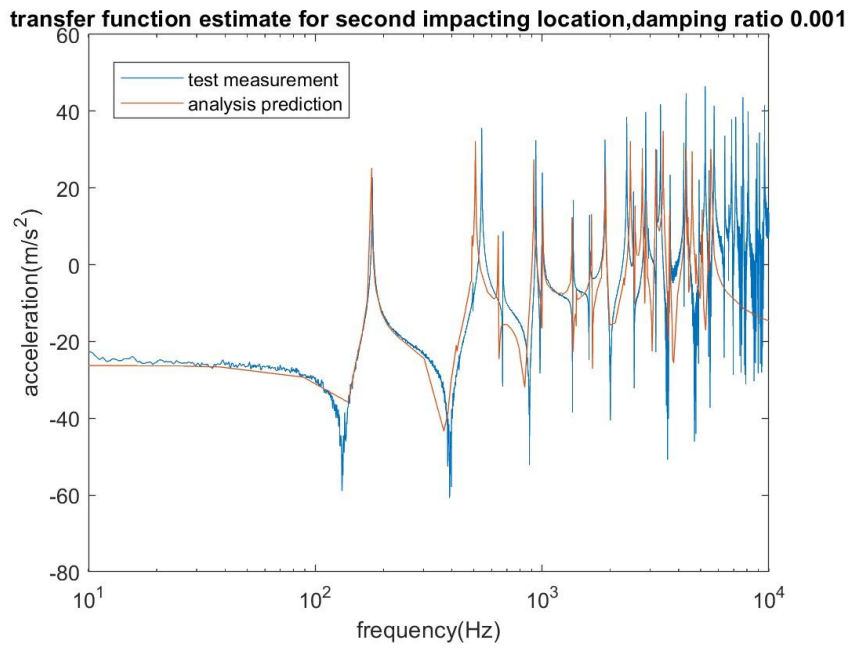
Figure 4.5 transfer function estimate for second impacting location, damping ratio 0.001
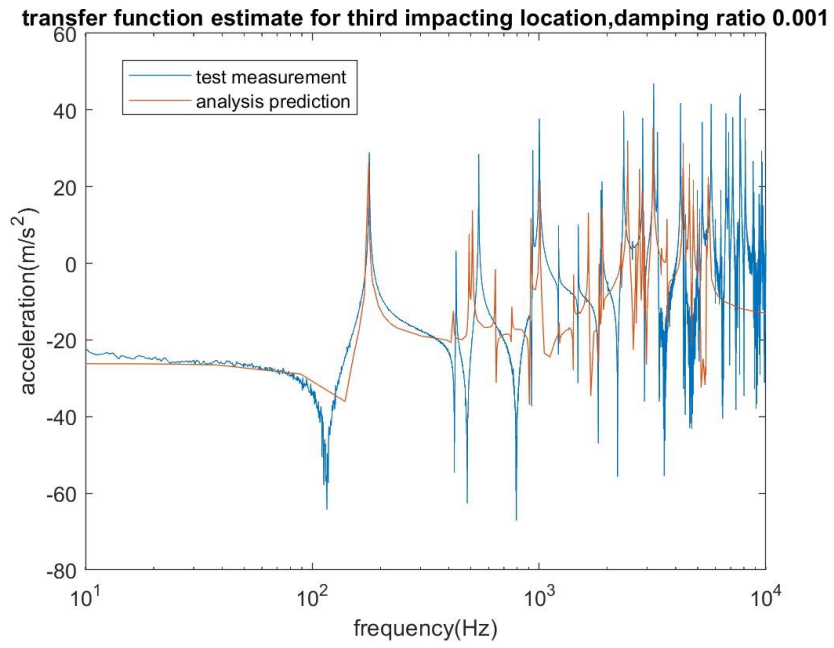
Figure 4.6 transfer function estimate for third impacting location, damping ratio 0.001

5 Conclusion

In this study, experimental tests were conducted to verify the impact force history and frequency response of small-scale pyroshock simulations. The accuracy of the predicted frequency history was validated by comparing it with experimental results. It was observed that the experimental results closely matched the predictions obtained through finite element analysis (FEA). Additionally, a sample pyrotechnic shock is tested by changing different condition including velocity, weight, tips and location, and the level of the shock is measured during its impact process.

Firstly, the effect of test system parameters on the half-sine force profile and the frequency response was observed by experimental tests. According to the study, an increase in weight causes more force to be exerted on the system in a force versus time diagram, so the response time of the system decreases.

To facilitate the initial design stage of a mechanical pyroshock simulation device that satisfies the required frequency response, an approximate method for predicting the impact force history is necessary. By employing this predicted impact force history, the resonant frequency can be determined. Subsequently, a resonant plate can be designed to match the anticipated frequency response. Moreover, the impactor's mass can be determined based on the correlation between the impact force history and various factors such as velocity, tips, and location. Employing these approaches for predicting the resonant frequency helps streamline the design process, saving both time and costs.

Appendix A - complete MATLAB codes

A.1 - Algorithm with Force-Time Relationship at the Center Point

```matlab
clc;                            %clear all variables from the
workspace
close;                          %clear all open figure windows

TEST=1;                         %assigns the values 1 to the
variables test

filename=['t' num2str(TEST) '.mat'];  % concatenates the string, the
                                        string representation of TEST,
                                      % create the filename string
load(filename)
N=length(Track1);               %calculates the length of the array
'Track 1 '
                                % and stores it in the variable 'N'
fs=Track1_TrueBandWidth*2.56;   % calculates the sampling
frequency
t=(0:length(Track1)-1)/fs;      %creates a time vector
[pks, locs] = findpeaks(Track1, t, 'SortStr', 'descend','NPeaks',4);
num_peaks = 4;
[locs,I] = sort(locs);
pks=pks(I);

% Find min
TTrack1=Track1;
TTrack1(Track1<10)=pks(1);
[pks2, locs2] = findpeaks(-TTrack1, t, 'SortStr', 'descend');
num_peaks2 = 8;
clear I
[locs2,I] = sort(locs2);
pks2=pks2(I);
clear I

% Plot data with peaks marked
figure
plot(t, Track1,'.')
hold on
scatter(locs(1:num_peaks), pks(1:num_peaks), 'ro')
```

```matlab
scatter(locs2(1:num_peaks2), -pks2(1:num_peaks2), 'ro')
xlabel('time [s]');
ylabel('Force [N]');

% Add text labels for each peak
for i = 1:num_peaks
    text(locs(i), pks(i), sprintf('(%.4f, %.4f)', locs(i), pks(i)),
'HorizontalAlignment', 'center', 'VerticalAlignment', 'bottom')
End

% Add text labels for each min
for i = 1:num_peaks2
    text(locs2(i), -pks2(i), sprintf('(%.4f, %.4f)', locs2(i), -pks2(i)),
'HorizontalAlignment', 'center', 'VerticalAlignment', 'bottom')
end
hold off

% Display x and y values of the marked peaks
disp('Peaks:')
for i = 1:num_peaks
    fprintf('t = %.4f, Track1 = %.4f\n', locs(i), pks(i))
End

% Display x and y values of the min
disp('Mins:')
for i = 1:num_peaks2
    fprintf('t = %.4f, Track1 = %.4f\n', locs2(i), pks2(i))
End

% CUT and COMPUTE FORCE CHARACTERISTICS
samp = 1:length(Track1);
scut = samp(Track1 > -1 & t>2.3535 & t<2.3543 );
Fcut = Track1(scut);
tcut = t(scut);
[Fmax, I] = max(Fcut);
T = tcut(end) - tcut(1);
tmax = tcut(I);
iL = trapz(tcut(1:I), Fcut(1:I));
iR = trapz(tcut(I:end), Fcut(I:end));
figure;
plot(tcut, Fcut);
xlabel('time [s]');
ylabel('Force [N]');
title('Force vs. Time');
```

```matlab
max_x = max(tcut);                          %Add axis maximum markers
max_y = max(Fcut);
y_threshold = Fmax/2;                       %Add time difference and left and
                                              right area markers

idx = find(Fcut > y_threshold);
if ~isempty(idx)
    x_left = tcut(idx(1));
    x_right = tcut(idx(end));
    y_left = trapz(tcut(1:idx(1)), Fcut(1:idx(1)));
    y_right = trapz(tcut(idx(end):end), Fcut(idx(end):end));
End

% add total time difference marker
text(max_x, max_y, [' Fmax = ', num2str(Fmax)], 'HorizontalAlignment',
'right', 'VerticalAlignment', 'top');
text(max_x, max_y*0.8, ['T = ', num2str(T)], 'HorizontalAlignment', 'right',
'VerticalAlignment', 'top');
text(max_x, max_y*0.9, ['tmax = ', num2str(tmax)], 'HorizontalAlignment',
'right', 'VerticalAlignment', 'top');
text(max_x, max_y*0.7, ['iL = ', num2str(iL)], 'HorizontalAlignment', 'right',
'VerticalAlignment', 'top');
text(max_x, max_y*0.6, ['iR = ', num2str(iR)], 'HorizontalAlignment', 'right',
'VerticalAlignment', 'top');
```

A.2 - Algorithm with Acceleration-Time Relationship at the Center Point

```matlab
clear;
clc;
close all;

TEST = 1;
filename = ['t' num2str(TEST) '.mat'];
load(filename);

fs = Track4_TrueBandWidth * 2.56;
t = (0:length(Track4)-1)/fs;

% Define window parameters
window_length = 3;
window_step = 1;
window_start = 0;
window_end = 10;
```

```matlab
% Create time windows
window_starts = window_start : window_step : (window_end -
window_length);
window_ends = window_starts + window_length;

% Find peaks for each window
pks_all = [];
locs_all = [];
for i = 1 : length(window_starts)
    % Find peaks within the window
    [pks, locs] = findpeaks(Track4(t >= window_starts(i) & t <
window_ends(i)), ...
        t(t >= window_starts(i) & t < window_ends(i)), 'SortStr', 'descend',
'NPeaks', 1);
    if ~isempty(pks) && ~isempty(locs)
    % Add peaks and locations to the arrays
        pks_all(end+1) = pks;
        locs_all(end+1) = locs;
    end
end

% Plot data with peaks marked
figure;
plot(t, Track4, 'k');
hold on;
scatter(locs_all, pks_all, 'ro', 'filled');
grid on

% Add text labels for each peak
for i = 1:length(pks_all)
    text(locs_all(i), pks_all(i), ['(' num2str(locs_all(i), '%.5f') ', '
num2str(pks_all(i), '%.5f') ')'], 'HorizontalAlignment', 'center',
'VerticalAlignment', 'bottom');
end

% Add labels and title
xlabel('Time [s]');
ylabel('Acceleration [m/s^2]');

% Display x and y values of the marked peaks
disp('Peaks:')
for i = 1:length(pks_all)
    fprintf('t = %.5f, Track3 = %.5f\n', locs_all(i), pks_all(i))
```

```matlab
end

% CUT and COMPUTE acceleration CHARACTERISTICS
samp=1:length(Track4);
scut = samp(Track4 > 0 & t>2.3774 & t<2.3778);
figure,plot(t(scut),Track4(scut))
grid on
xlabel('time [s]')
legend('Acceleration [m/s^2]')
Acut=Track4(scut);
tcut=(0:length(Acut)-1)/fs;
[Amax, I]=max(Acut);
format long
T=tcut(end);
Amax;
tmax=tcut(I);
iL=trapz(tcut(1:I),Acut(1:I));
iR=trapz(tcut(I:end),Acut(I:end));
check=trapz(tcut,Acut)-iL-iR;            %(must be 0)
A=[Amax T tmax iL iR check];
writematrix(A, 'acceleration.xlsx', 'Sheet', 1, 'Range', 'A8');
```

A.3 - Using Fast Fourier Transform Algorithm for sensors

```matlab
clear all;
clc;
close all

TEST = 1;
filename = ['t' num2str(TEST) '.mat'];
load(filename);

N=length(Track1);                        %calculates the length of the array
'Track 1 '
fs=Track1_TrueBandWidth*2.56;            % calculates the sampling
frequency
t=(0:length(Track1)-1)/fs;               %creates a time vector
freq= 0:(1/t(end)):fs/2-(1/t(end));

FFT4 =fft(Track4,N)*(2/N);
abs_Track4=abs(FFT4);

FFT7 =fft(Track7,N)*(2/N);
```

```
abs_Track7=abs(FFT7);

FFT9 =fft(Track9,N)*(2/N);
abs_Track9=abs(FFT9);

FFT13=fft(Track13,N)*(2/N);
abs_Track13=abs(FFT13);

FFT16=fft(Track16,N)*(2/N);
abs_Track16=abs(FFT16);

FFT19=fft(Track19,N)*(2/N);
abs_Track19=abs(FFT19);

FFT20=fft(Track20,N)*(2/N);
abs_Track20=abs(FFT20);

FFT21=fft(Track21,N)*(2/N);
abs_Track21=abs(FFT21);

FFT22 =fft(Track22,N)*(2/N);
abs_Track22=abs(FFT22);

FFT23=fft(Track23,N)*(2/N);
abs_Track23=abs(FFT23);

FFT24=fft(Track24,N)*(2/N);
abs_Track24=abs(FFT24);

ABS=abs_Track4+abs_Track7+abs_Track9+abs_Track13+abs_Track16+abs_
Track19+abs_Track20+abs_Track21+abs_Track22+abs_Track23+abs_Track
24;

figure;loglog(freq,ABS(1:length(freq))), xlim([1e2 1e4])
```

A.4 - Using Transfer Function Estimate Algorithm for all sensors

```
clear all;
clc;
close all

TEST = 1;
filename = ['t' num2str(TEST) '.mat'];
```

```matlab
load(filename);

N_Track1=length(Track1);                %calculates the length of the
array 'Track 1 '
fs=Track1_TrueBandWidth*2.56;           % calculates the sampling
frequency
t=(0:length(Track1)-1)/fs;              %creates a time vector

M=floor(N_Track1/4);
tfwindow= M;                            %dimension of the window
NFFT =M;                                % sampling point, set the number
of the points
tfnoverlap = floor(.9*M);               % overlap of the windows
[Tf,f]=tfestimate(Track1,Track4,tfwindow,tfnoverlap,NFFT,fs);
[Tfc,fc]=mscohere(Track1,Track4,tfwindow,tfnoverlap,NFFT,fs);

figure;
[pxx1,f] = pwelch(Track1,tfwindow,tfnoverlap,NFFT,fs);
[pxx,f] = pwelch(Track4,tfwindow,tfnoverlap,NFFT,fs);
loglog(f,pxx1), hold on, loglog(f,pxx)

figure,
subplot(3,1,1)
plot(f,20*log10(abs(Tf)),'-')
set(gca,'xscale','log')
xlim([0 10000])
xlabel('frequency[Hz]')
ylabel('Mag[dB]')

subplot(3,1,2)
plot(f,angle(Tf).*180/pi,'-')
set(gca,'xscale','log')
  xlim([0 10000])
xlabel('frequency[Hz]')
ylabel('Phase[deg]')

subplot(3,1,3)
plot(fc,Tfc)
set(gca,'xscale','log')
xlim([0 10000])
xlabel('frequency[Hz]');
ylabel('coherence');
ytickformat('%.0f');
```

A.4 – Compare with SOLIDWORKS using Transfer Function Estimate Algorithm for all sensors

```
filename = 'Response Graph-4.csv ';
sheet = '1';
range1 = 'B10:B143';
range2 = 'C10:C143';

data1 = readmatrix(filename,    'Range', range1);
data2 = readmatrix(filename,    'Range', range2);

figure

semilogx(data1,20*log10(abs(data2))),
xlim([1e1 1e4])
xlabel('frequency(Hz)')
ylabel('acceleration(m/s^2)')
grid on

figure;
semilogx(f,20*log10(abs(Tf)),'-'), hold on
semilogx(data1,20*log10(abs(data2))),
xlim([1e1 1e4])
xlabel('frequency(Hz)')
ylabel('acceleration(m/s^2)')
```

A.5 – prony test algorithm

```
%% prony shape
clear all
close all
clc

TEST = 1;
filename = ['t' num2str(TEST) '.mat'];
load(filename);

N=length(Track1);
fs=Track1_TrueBandWidth*2.56;
ind1=241025;
ind2=441025;
```

```matlab
y1=Track4(ind1:ind2);
y2=Track7(ind1:ind2);
y3=-Track9(ind1:ind2);
y4=Track13(ind1:ind2);
y5=Track16(ind1:ind2);
y6=Track19(ind1:ind2);
y7=Track20(ind1:ind2);
y8=Track21(ind1:ind2);
y9=Track22(ind1:ind2);
y10=Track23(ind1:ind2);
y11=Track24(ind1:ind2);

%Beam & Acc location
X=[300      300      300      400      400      400      500      200
200      200    100];
Y=[175      85       270      85       175      270      175      85
175      270    175];

%%% Spectra
NFFT=2^nextpow2(N);
YYY=0;
for j=1:11
    eval(['y=y' num2str(j) ';'])
    YY=fft(y,NFFT)./N;
    YY(2:end)=2*YY(2:end);
    YYY=YYY+abs(YY);
end
ff=[0:NFFT-1]*fs/NFFT;
figure;plot(ff,YYY), xlim([40 200]), xlabel('f [Hz]'), ylabel('acc. amplitude
sum')
title('Prony Stabilization Diagram')
%%% decimate to reduce fs
r=200;
fs=fs/r;
for j=1:11
    eval(['y' num2str(j) '=decimate(y' num2str(j)    ',r);'])
end
N=length(y1);

%%% prony stabilization
for k=20:100
    [FREQ, DAM, COEF]=my_prony(y1,1/fs,k);
    hold on, plot(FREQ,(0.01+0.05*k)*ones(size(FREQ)),'m.')
end
```

```matlab
%% 178.4: rough estimate of 1st mode from spectrum
for m=1:11
    eval(['[FREQ, DAM, COEF]=my_prony(y' num2str(m) ',1/fs,k);'])
    [M in]=min(abs(FREQ-178.4));
    eval(['f1_' num2str(m) '=FREQ(in);'])
    eval(['d1_' num2str(m) '=DAM(in);'])
    eval(['A1_' num2str(m) '=COEF(in);'])
end

f1_est=mean([f1_1,f1_2,f1_3,f1_4,f1_5,f1_6,f1_7,f1_8,f1_9,f1_10,f1_11])
d1_est=mean([d1_1,d1_2,d1_3,d1_4,d1_5,d1_6,d1_7,d1_8,d1_9,d1_10,d1_11])

A1=A1_1/A1_1;
A2=A1_2/A1_1;
A3=A1_3/A1_1;
A4=A1_4/A1_1;
A5=A1_5/A1_1;
A6=A1_6/A1_1;
A7=A1_7/A1_1;
A8=A1_8/A1_1;
A9=A1_9/A1_1;
A10=A1_10/A1_1;
A11=A1_11/A1_1;
a1=angle(A1)*180/pi
Z=[abs(A1),abs(A2),abs(A3),abs(A4),abs(A5),abs(A6),abs(A7),abs(A8),abs(A9)
,abs(A10),abs(A11)];
figure;plot3(X,Y,Z,'.'),grid on
hold on;quiver3(X,Y,zeros(size(X)),zeros(size(X)),zeros(size(X)),Z,'off')
title(['Prony Estimate of First Modal Shape - f1='
num2str(floor(f1_est*100)/100) 'Hz, \zeta =' num2str(floor(d1_est*100)/100)])
view(-5,16)
```

A.6 – FEM test algorithm

```matlab
clear;
close all;
clc ;

%% Disc Model Definition
a=0.600;
b=0.360;
h=0.012;
```

```matlab
r=0.005;
gm = multicuboid([r a],[r b],h);
hmax = h/2;                                      %for mesh size

%%%MATERIAL: PLAIN STEEL
E=2.1E11;                                         %Pa
v=0.3;                                            %Poisson
ro=7800;                                          %kg/m3

%%% Analytic sol, Blevins
i=3;
j=1;
Lam2=pi^2*(GG(i)^4+(a/b)^4*GG(j)^4+2*(a/b)^2*(JJ(i)*JJ(j)+2*v*(HH(i)*
HH(j)-JJ(i)*JJ(j))))^.5;
f=Lam2/(2*pi*a^2)*(E*h^2/(12*ro*(1-v^2)))^.5;

%%% MODAL analysis settings
model = createpde("structural","modal-solid");
model.Geometry =gm;
figure(1)
subplot(1,3,1),pdegplot(model,"CellLabels","on","FaceAlpha",0.5),title('Cells
')
subplot(1,3,2),pdegplot(model,"FaceLabels","on","FaceAlpha",0.5),title('Fac
es')

%%%%MESH
msh = generateMesh(model,'Hmax',hmax);
figure(1)
subplot(1,3,3),pdemesh(model),title('Mesh')

%%MATERIAL (Plain Carbon Steel)
structuralProperties(model,"YoungsModulus",E, ...
                          "PoissonsRatio",v, ...
                          "MassDensity",ro);

%%BC
structuralBC(model,"Face",1,"Constraint","free");

%%% SOLVE modal
modalresults = solve(model,'FrequencyRange',[10,300]*2*pi);
modalresults.NaturalFrequencies/(2*pi);

figure;
subplot(1,3,1)
```

```matlab
pdeplot3D(modalresults.Mesh,'ColorMapData',modalresults.ModeShapes.uz(:
,1))
title(['Mode with Frequency ', ...
        num2str(floor(modalresults.NaturalFrequencies(1)/(2*pi))),' Hz'])
axis equal
subplot(1,3,2)
pdeplot3D(modalresults.Mesh,'ColorMapData',modalresults.ModeShapes.uz(:
,2))
title(['Mode with Frequency ', ...
        num2str(floor(modalresults.NaturalFrequencies(2)/(2*pi))),' Hz'])
axis equal
subplot(1,3,3)
pdeplot3D(modalresults.Mesh,'ColorMapData',modalresults.ModeShapes.uz(:
,3))
title(['Mode with Frequency ', ...
        num2str(floor(modalresults.NaturalFrequencies(3)/(2*pi))),' Hz'])
axis equal

%% CREATE and SOLVE frf
modelFR = createpde("structural","frequency-solid");
modelFR.Geometry =gm;
msh = generateMesh(modelFR,'Hmax',hmax);
structuralProperties(modelFR,"YoungsModulus",E, ...
                                "PoissonsRatio",v, ...
                                "MassDensity",ro);
structuralBC(modelFR,"Face",1,"Constraint","free");
structuralBoundaryLoad(modelFR,"Face",1,"Pressure",1E0/(pi*r^2));

flist = [logspace(1.5,2.5,100)]*2*pi;
FRFresults = solve(modelFR,flist);
iAccU = interpolateAcceleration(FRFresults,[0;0;h]);          %Track4
iAccU2 = interpolateAcceleration(FRFresults,[0;0.075;h]);      %Track7
iAccU3 = interpolateAcceleration(FRFresults,[.1;0.075;h]);    %Track13
figure
semilogx(FRFresults.SolutionFrequencies/(2*pi),20*log10(abs(iAccU.uz)));
xlabel('f [Hz]')
ylabel('acc [m / _{s^2}] dB')
title("Magnitude")
grid on
xlim([10^1.5 10^2.5])
ylim([0 0.5])

%% FUN
function g=GG(x)
```

```matlab
    if x==1 || x==2
        g=0;
    elseif x==3
        g=1.506;
    else
        g=x-3/2;
    end
end

function h=HH(x)
    if x==1
        h=0;
    elseif x==2
        h=1.248;
    elseif x==3
        h=1.506;
    else
        h=(x-3/2)*(1-2*(pi*(x-3/2))^-1);
    end
end

function j=JJ(x)
    if x==1
        j=0;
    elseif x==2
        j=1.216;
    elseif x==3
        j=5.017;
    else
        j=(x-3/2)^2*(1+6*(pi*(x-3/2))^-1);
    end
end
```

Appendix B – figure and tables indexes

B.1 - the data for different cases

A: hammer speed   **(0,1 -- low speed, high speed)** ,
B : additional weight   **(0,1 -- aluminium, Ferrum)**
C: hammer tip material   **(0,1,2 -- rubber tip, flat metal tip , round metal tip)**
D: location   **(center, +x, +2x,+y, +2y)**

RUN	COMBINATION	FACTOR				weight	
		A	B	C	D		
1	.(1)	0	0	0	center (29.7,17.5)	aluminum + rubber = 33 g	Light
2	a	1	0	0	center (29.7,17.5)	aluminum + rubber = 33 g	
3	.(1)	0	0	0	.+x (39.7,17.5)	aluminum + rubber = 33 g	
4	a	1	0	0	.+x (39.7,17.5)	aluminum + rubber = 33 g	
5	.(1)	0	0	0	.+y (29.7,8.5)	aluminum + rubber = 33 g	
6	a	1	0	0	.+y (29.7,8.5)	aluminum + rubber = 33 g	
7	.(1)	0	0	0	.+xy (39.7,8.5)	aluminum + rubber = 33 g	
8	a	1	0	0	.+xy (39.7,8.5)	aluminum + rubber = 33 g	
9	.(1)	0	0	0	.+2x (49.7,17.5)	aluminum + rubber = 33 g	
10	a	1	0	0	.+2x (49.7,17.5)	aluminum + rubber = 33 g	
11	b	0	1	0	center (29.7,17.5)	iron + rubber = 85 g	Heavy
12	ab	1	1	0	center (29.7,17.5)	iron + rubber = 85 g	
13	b	0	1	0	.+x (39.7,17.5)	iron + rubber = 85 g	
14	ab	1	1	0	.+x (39.7,17.5)	iron + rubber = 85 g	
15	b	0	1	0	.+y (29.7,8.5)	iron + rubber = 85 g	
16	ab	1	1	0	.+y (29.7,8.5)	iron + rubber = 85 g	
17	b	0	1	0	.+xy (39.7,8.5)	iron + rubber = 85 g	
18	ab	1	1	0	.+xy (39.7,8.5)	iron + rubber = 85 g	

19	b	0	1	0	.+2x (49.7,17.5)	iron + rubber = 85 g	
20	ab	1	1	0	.+2x (49.7,17.5)	iron + rubber = 85 g	
21	c	0	0	1	center (29.7,17.5)	aluminum + flat = 38 g	Light
22	ac	1	0	1	center (29.7,17.5)	aluminum + flat = 38 g	
23	c	0	0	1	.+x (39.7,17.5)	aluminum + flat = 38 g	
24	ac	1	0	1	.+x (39.7,17.5)	aluminum + flat = 38 g	
25	c	0	0	1	.+y (29.7,8.5)	aluminum + flat = 38 g	
26	ac	1	0	1	.+y (29.7,8.5)	aluminum + flat = 38 g	
27	c	0	0	1	.+xy (39.7,8.5)	aluminum + flat = 38 g	
28	ac	1	0	1	.+xy (39.7,8.5)	aluminum + flat = 38 g	
29	c	0	0	1	.+2x (49.7,17.5)	aluminum + flat = 38 g	
30	ac	1	0	1	.+2x (49.7,17.5)	aluminum + flat = 38 g	
31	bc	0	1	1	center (29.7,17.5)	iron + flat = 90 g	Heavy
32	abc	1	1	1	center (29.7,17.5)	iron + flat = 90 g	
33	bc	0	1	1	.+x (39.7,17.5)	iron + flat = 90 g	
34	abc	1	1	1	.+x (39.7,17.5)	iron + flat = 90 g	
35	bc	0	1	1	.+y (29.7,8.5)	iron + flat = 90 g	
36	abc	1	1	1	.+y (29.7,8.5)	iron + flat = 90 g	
37	bc	0	1	1	.+xy (39.7,8.5)	iron + flat = 90 g	
38	abc	1	1	1	.+xy (39.7,8.5)	iron + flat = 90 g	
39	bc	0	1	1	.+2x (49.7,17.5)	iron + flat = 90 g	
40	abc	1	1	1	.+2x (49.7,17.5)	iron + flat = 90 g	
41	d	0	~	2	center (29.7,17.5)	round =65 g	Light
42	ad	1	~	2	center (29.7,17.5)	round =65 g	
43	d	0	~	2	.+x (39.7,17.5)	round =65 g	
44	ad	1	~	2	.+x (39.7,17.5)	round =65 g	
45	d	0	~	2	.+y (29.7,8.5)	round =65 g	
46	ad	1	~	2	.+y (29.7,8.5)	round =65 g	
47	d	0	~	2	.+xy (39.7,8.5)	round =65 g	
48	ad	1	~	2	.+xy (39.7,8.5)	round =65 g	

49	d	0	~	2	.+2x (49.7,17.5)	round =65 g	
50	ad	1	~	2	.+2x (49.7,17.5)	round =65 g	
51	bd	0	1	2	center (29.7,17.5)	aluminum + round = 93 g	
52	abd	1	1	2	center (29.7,17.5)	aluminum + round = 93 g	
53	bd	0	1	2	.+x (39.7,17.5)	aluminum + round = 93 g	
54	abd	1	1	2	.+x (39.7,17.5)	aluminum + round = 93 g	
55	bd	0	1	2	.+y (29.7,8.5)	aluminum + round = 93 g	Heavy
56	abd	1	1	2	.+y (29.7,8.5)	aluminum + round = 93 g	
57	bd	0	1	2	.+xy (39.7,8.5)	aluminum + round = 93 g	
58	abd	1	1	2	.+xy (39.7,8.5)	aluminum + round = 93 g	
59	bd	0	1	2	.+2x (49.7,17.5)	aluminum + round = 93 g	
60	abd	1	1	2	.+2x (49.7,17.5)	aluminum + round = 93 g	

B.2 - The data for the force measurements

number	Impact number	Fmax(N)	Tmax(S)	Δt(s)	Δt_left(s)	left area (N*s)	right area (N*s)	totally area (N*s)	restitution coefficient
t1	t1-1	235.8161	2.3540	4.9805E-04	2.5391E-04	0.0347	0.0345	0.0693	0.4985
	t1-2	279.3109	4.3977	4.8828E-04	1.9531E-04	0.0385	0.0439	0.0824	0.5326
	t1-3	375.8254	6.6607	4.6875E-04	2.3438E-04	0.0512	0.0554	0.1066	0.5199
	t1-4	442.0471	9.1890	4.7852E-04	2.5391E-04	0.0619	0.0634	0.1253	0.5058
t2	t2-1	670.7101	2.5539	3.9063E-04	1.8555E-04	0.0810	0.0935	0.1745	0.5360
	t2-2	585.5712	4.7296	4.6875E-04	2.0508E-04	0.0780	0.0810	0.1590	0.5093
	t2-3	646.2350	6.7853	4.6875E-04	2.0508E-04	0.0855	0.0910	0.1765	0.5155
	t2-4	753.3681	9.0696	4.7852E-04	2.1484E-04	0.0976	0.1040	0.2016	0.5158
t3	t3-1	315.4279	2.0539	4.7852E-04	2.0508E-04	0.0402	0.0463	0.0866	0.5353
	t3-2	365.5366	4.0229	4.6875E-04	1.8555E-04	0.0450	0.0554	0.1004	0.5520
	t3-3	492.9067	5.9781	3.9063E-04	1.7578E-04	0.0614	0.0661	0.1275	0.5182
	t3-4	502.8966	7.9813	2.9297E-04	2.3438E-04	0.0634	0.0283	0.0917	0.3084
t4	t4-1	597.8787	2.4755	4.7852E-04	2.1484E-04	0.0776	0.0824	0.1600	0.5153
	t4-2	640.7916	4.3617	4.7852E-04	1.9531E-04	0.0779	0.0945	0.1724	0.5482
	t4-3	638.7474	6.2336	4.7852E-04	2.0508E-04	0.0826	0.0880	0.1707	0.5157
	t4-4	867.2153	8.1578	3.9063E-04	1.7578E-04	0.1032	0.1140	0.2171	0.5249
t5	t5-1	403.4285	2.0210	3.9063E-04	1.7578E-04	0.0490	0.0582	0.1072	0.5429
	t5-2	404.3913	3.7672	4.5898E-04	1.8555E-04	0.0504	0.0597	0.1100	0.5423
	t5-3	409.4936	5.7940	4.7852E-04	1.9531E-04	0.0521	0.0588	0.1109	0.5299
	t5-4	520.7382	7.6224	4.7852E-04	1.9531E-04	0.0614	0.0749	0.1363	0.5496
t6	t6-1	720.4290	1.7090	4.6875E-04	2.1484E-04	0.0880	0.0946	0.1826	0.5182
	t6-2	787.3804	3.5635	3.9063E-04	1.8555E-04	0.0948	0.1012	0.1960	0.5164
	t6-3	719.0794	5.3911	3.9063E-04	1.6602E-04	0.0852	0.0956	0.1809	0.5289
	t6-4	967.8900	7.1478	3.8086E-04	2.0508E-04	0.1132	0.1167	0.2299	0.5078
t7	t7-1	426.4288	1.5878	3.9063E-04	1.6602E-04	0.0511	0.0630	0.1140	0.5523

	t7-2	571.4146	3.4622	4.6875E-04	2.0508E-04	0.0719	0.0767	0.1486	0.5160
	t7-3	640.6267	5.3460	3.9063E-04	1.5625E-04	0.0718	0.0906	0.1624	0.5579
	t7-4	667.8579	7.0988	3.9063E-04	1.5625E-04	0.0771	0.0899	0.1670	0.5384
t8	t8-1	1010.8883	1.7618	4.7852E-04	2.0508E-04	0.1183	0.1318	0.2501	0.5270
	t8-2	804.5713	4.0986	4.5898E-04	2.0508E-04	0.0952	0.1147	0.2100	0.5465
	t8-3	895.6370	6.7625	4.5898E-04	2.1484E-04	0.1063	0.1223	0.2286	0.5349
	t8-4	1178.8270	9.1423	3.8086E-04	1.5625E-04	0.1313	0.1349	0.2662	0.5067
t9	t9-1	493.4235	1.8568	4.7852E-04	2.0508E-04	0.0616	0.0727	0.1343	0.5415
	t9-2	614.2065	3.9111	3.9063E-04	1.8555E-04	0.0788	0.0821	0.1609	0.5100
	t9-3	495.6462	5.7645	4.8828E-04	2.2461E-04	0.0643	0.0725	0.1367	0.5300
	t9-4	689.3022	7.6537	4.5898E-04	2.1484E-04	0.0883	0.0962	0.1845	0.5212
t10	t10-1	856.7610	2.0398,	3.8086E-04	1.6602E-04	0.0986	0.1155	0.2141	0.5396
	t10-2	1052.9500	4.2348,	4.5898E-04	2.0508E-04	0.1195	0.1368	0.2563	0.5338
	t10-3	881.8179	6.6812,	3.9063E-04	1.5625E-04	0.0983	0.1217	0.2199	0.5532
	t10-4	1389.8761	8.6671,	3.8086E-04	1.4648E-04	0.1433	0.1515	0.2948	0.5138
t11	t11-1	572.2746	2.0387	6.8617E-04	3.7344E-04	0.0929	0.1050	0.1979	0.5306
	t11-2	828.3776	4.3256	4.9086E-04	1.9648E-04	0.0872	0.1152	0.2024	0.5692
	t11-3	753.0155	6.3875	6.7828E-04	2.6461E-04	0.1035	0.1098	0.2133	0.5148
	t11-4	938.9379	8.6780	5.9828E-04	2.0531E-04	0.1253	0.1258	0.2511	0.5010
t12	t12-1	1550.4170	2.0587	4.6878E-04	2.6590E-04	0.2011	0.2057	0.4068	0.5057
	t12-2	1035.0215	4.8925	5.3678E-04	2.5698E-04	0.1430	0.1502	0.2932	0.5123
	t12-3	1452.4982	6.3985	4.6552E-04	2.3659E-04	0.1968	0.1901	0.3869	0.4913
	t12-4	1236.4717	9.1250	3.8453E-04	2.3659E-04	0.1283	0.1302	0.2585	0.5037
t13	t13-1	592.2746	2.7269,	5.7617E-04	2.7344E-04	0.0919	0.1032	0.1951	0.5289
	t13-2	728.3776	4.6948,	3.8086E-04	1.4648E-04	0.0880	0.1177	0.2057	0.5722
	t13-3	674.0155	6.8223,	4.8828E-04	2.2461E-04	0.1036	0.1087	0.2123	0.5120
	t13-4	818.9379	9.0247,	4.8828E-04	1.9531E-04	0.1150	0.1275	0.2425	0.5258
t14	t14-1	1650.4170	1.9980,	4.7852E-04	2.1484E-04	0.1955	0.2144	0.4100	0.5231
	t14-2	1019.0214	4.3374,	5.4688E-04	2.4414E-04	0.1388	0.1592	0.2981	0.5342
	t14-3	1478.4694	6.5277,	4.7852E-04	2.1484E-04	0.1867	0.1881	0.3748	0.5019

	t14-4	1267.3217	8.5311,	3.9063E-04	2.2461E-04	0.1781	0.1446	0.3227	0.4480
t15	t15-1	529.0920	1.6751,	4.8828E-04	2.4414E-04	0.0813	0.0842	0.1655	0.5086
	t15-2	503.8410	3.8874,	5.8594E-04	2.6367E-04	0.0782	0.0842	0.1624	0.5185
	t15-3	726.5688	5.8340,	4.9805E-04	2.5391E-04	0.1092	0.1091	0.2182	0.4998
	t15-4	788.6522	7.8484,	5.2734E-04	2.5391E-04	0.1133	0.1251	0.2385	0.5248
t16	t16-1	864.8495	0.9976,	4.8828E-04	2.4414E-04	0.1247	0.1355	0.2602	0.5206
	t16-2	1328.6381	3.0625,	4.7852E-04	2.4414E-04	0.1833	0.1711	0.3544	0.4829
	t16-3	1035.6315	5.2632,	4.8828E-04	1.9531E-04	0.1377	0.1588	0.2965	0.5356
	t16-4	1587.7706	7.5024,	4.7852E-04	2.0508E-04	0.1983	0.2018	0.4001	0.5043
t17	t17-1	715.8398	1.7051,	4.8828E-04	2.0508E-04	0.1073	0.1052	0.2125	0.4949
	t17-2	839.0374	3.8197,	4.8828E-04	2.1484E-04	0.1235	0.1243	0.2479	0.5016
	t17-3	879.0999	6.0591,	4.8828E-04	2.3438E-04	0.1291	0.1297	0.2588	0.5011
	t17-4	931.8940	8.3681,	4.9805E-04	2.4414E-04	0.1336	0.1404	0.2740	0.5123
t18	t18-1	1367.6387	2.0348,	4.8828E-04	2.1484E-04	0.1788	0.1783	0.3571	0.4993
	t18-2	1489.7067	3.9688,	3.9063E-04	1.7578E-04	0.1769	0.1889	0.3658	0.5164
	t18-3	1076.8104	6.2886,	5.3711E-04	2.5391E-04	0.1517	0.1519	0.3037	0.5003
	t18-4	965.0757	8.2542,	6.1523E-04	2.4414E-04	0.1377	0.1479	0.2856	0.5179
t19	t19-1	690.5533	2.0451,	5.6641E-04	2.5391E-04	0.1075	0.1121	0.2195	0.5105
	t19-2	717.8859	4.4318,	4.9805E-04	2.4414E-04	0.1048	0.1146	0.2194	0.5225
	t19-3	802.2007	6.5577,	5.5664E-04	2.5391E-04	0.1152	0.1306	0.2458	0.5314
	t19-4	856.7598	8.8738,	5.9570E-04	2.5391E-04	0.1255	0.1376	0.2631	0.5230
t20	t20-1	1483.9561	1.4213,	4.8828E-04	2.3438E-04	0.2008	0.1824	0.3833	0.4760
	t20-2	1629.3352	3.6851,	3.9063E-04	1.6602E-04	0.1849	0.2090	0.3938	0.5306
	t20-3	1509.8916	6.1738,	4.6875E-04	2.4414E-04	0.1884	0.1969	0.3853	0.5111
	t20-4	1785.7832	8.5783,	3.9063E-04	1.7578E-04	0.2002	0.2225	0.4227	0.5264
t21	t21-1	1322.3654	1.6791,	2.9297E-04	9.7656E-05	0.0508	0.0547	0.1055	0.5182
	t21-2	1406.8624	3.9238,	3.0273E-04	9.7656E-05	0.0524	0.0602	0.1126	0.5348
	t21-3	1282.1902	6.4099,	1.8555E-04	8.7891E-05	0.0462	0.0540	0.1003	0.5389
	t21-4	1424.8660	8.6701,	3.6133E-04	9.7656E-05	0.0498	0.0656	0.1154	0.5687
t22	t22-1	1259.1981	2.3538,	3.5156E-04	7.8125E-05	0.0482	0.0551	0.1033	0.5333

	t22-2	1758.2756	4.7156,	3.7109E-04	1.1719E-04	0.0555	0.0829	0.1384	0.5989
	t22-3	1935.9253	7.3231,	3.4180E-04	1.0742E-04	0.0684	0.0797	0.1481	0.5382
	t22-4	1987.6190	9.9031,	3.6133E-04	1.1719E-04	0.0629	0.0931	0.1559	0.5968
t23	t23-1	1132.5393	2.8168,	3.2227E-04	6.8359E-05	0.0373	0.0562	0.0935	0.6010
	t23-2	1117.5925	5.0921,	3.2227E-04	7.8125E-05	0.0384	0.0571	0.0955	0.5979
	t23-3	1289.0905	7.4377,	3.0273E-04	9.7656E-05	0.0453	0.0605	0.1058	0.5718
	t23-4	1151.1884	9.3177,	3.5156E-04	7.8125E-05	0.0365	0.0641	0.1006	0.6375
t24	t24-1	1511.4825	1.3562,	3.1250E-04	9.7656E-05	0.0589	0.0635	0.1223	0.5187
	t24-2	1499.0748	3.4291,	3.5156E-04	8.7891E-05	0.0452	0.0763	0.1214	0.6280
	t24-3	1881.6765	5.2845,	3.2227E-04	1.0742E-04	0.0619	0.0830	0.1449	0.5726
	t24-4	1984.5901	7.2218,	3.4180E-04	1.0742E-04	0.0746	0.0826	0.1572	0.5253
t25	t25-1	1101.5685	1.6937,	3.6133E-04	9.7656E-05	0.0342	0.0604	0.0946	0.6380
	t25-2	1005.1934	3.9364,	3.7109E-04	8.7891E-05	0.0382	0.0491	0.0872	0.5624
	t25-3	932.3199	6.4361,	3.2227E-04	9.7656E-05	0.0367	0.0446	0.0813	0.5487
	t25-4	1040.6311	8.6479,	3.9063E-04	7.8125E-05	0.0370	0.0542	0.0913	0.5944
t26	t26-1	832.0765	1.4023,	3.1250E-04	8.7891E-05	0.0336	0.0406	0.0741	0.5470
	t26-2	923.3736	3.4039,	3.8086E-04	8.7891E-05	0.0336	0.0509	0.0845	0.6021
	t26-3	1803.2007	5.9044,	3.6133E-04	1.0742E-04	0.0557	0.0877	0.1434	0.6113
	t26-4	2046.1638	8.0248,	3.3203E-04	1.0742E-04	0.0636	0.0945	0.1581	0.5979
t27	t27-1	691.6454	1.6186,	3.4180E-04	7.8125E-05	0.0285	0.0365	0.0650	0.5611
	t27-2	1194.4399	3.9512,	3.4180E-04	8.7891E-05	0.0362	0.0641	0.1003	0.6389
	t27-3	985.5246	6.0194,	3.3203E-04	9.7656E-05	0.0312	0.0529	0.0841	0.6293
	t27-4	1120.3184	8.0240,	3.2227E-04	7.8125E-05	0.0393	0.0563	0.0956	0.5890
t28	t28-1	1700.8484	1.0290,	3.0273E-04	1.0742E-04	0.0671	0.0692	0.1362	0.5076
	t28-2	1265.0254	3.0061,	2.8320E-04	5.8594E-05	0.0430	0.0603	0.1033	0.5841
	t28-3	1535.3757	4.9494,	3.6133E-04	8.7891E-05	0.0502	0.0761	0.1262	0.6027
	t28-4	1708.4855	6.7414,	2.8320E-04	6.8359E-05	0.0585	0.0794	0.1379	0.5756
t29	t29-1	1001.3060	1.8037,	2.9297E-04	6.8359E-05	0.0374	0.0480	0.0854	0.5621
	t29-2	928.4883	3.9032,	3.3203E-04	8.7891E-05	0.0318	0.0502	0.0820	0.6121
	t29-3	737.4437	6.0021,	3.6133E-04	1.3672E-04	0.0357	0.0344	0.0701	0.4906

	t29-4	1068.5392	8.0006,	3.0273E-04	7.8125E-05	0.0364	0.0536	0.0900	0.5958
t30	t30-1	1981.4312	1.7705,	3.2227E-04	1.1719E-04	0.0611	0.0958	0.1569	0.6106
	t30-2	1373.8894	4.3119,	3.7109E-04	9.7656E-05	0.0522	0.0611	0.1133	0.5393
	t30-3	1571.5597	6.5388,	3.1250E-04	9.7656E-05	0.0586	0.0713	0.1299	0.5492
	t30-4	1747.7750	8.6088,	3.4180E-04	1.1719E-04	0.0568	0.0842	0.1410	0.5973
t31	t31-1	910.6656	1.9510,	2.9297E-04	6.8359E-05	0.0320	0.0530	0.0850	0.6231
	t31-2	1591.8365	4.3474,	2.8320E-04	5.8594E-05	0.0508	0.0800	0.1307	0.6117
	t31-3	1076.2837	6.6086,	2.6367E-04	5.8594E-05	0.0371	0.0532	0.0904	0.5890
	t31-4	856.5201	8.9413,	3.4180E-04	9.7656E-05	0.0397	0.0370	0.0766	0.4824
t32	t32-1	856.2140	1.4118,	3.5156E-04	1.0742E-04	0.0320	0.0438	0.0759	0.5777
	t32-2	1113.9531	3.0860,	3.3203E-04	6.8359E-05	0.0395	0.0539	0.0934	0.5769
	t32-3	960.9321	5.1661,	3.2227E-04	1.0742E-04	0.0371	0.0466	0.0837	0.5565
	t32-4	1202.9141	6.9593,	3.1250E-04	9.7656E-05	0.0448	0.0545	0.0992	0.5490
t33	t33-1	742.6036	1.8146,	3.4180E-04	9.7656E-05	0.0379	0.0312	0.0691	0.4512
	t33-2	796.6797	3.6351,	3.4180E-04	8.7891E-05	0.0377	0.0381	0.0758	0.5026
	t33-3	832.2438	5.5886,	3.5156E-04	8.7891E-05	0.0292	0.0481	0.0772	0.6224
	t33-4	1166.8185	7.6064,	2.7344E-04	5.8594E-05	0.0359	0.0631	0.0990	0.6372
t34	t34-1	954.4191	1.6921,	3.3203E-04	1.0742E-04	0.0351	0.0515	0.0866	0.5947
	t34-2	1194.7140	3.4259,	3.0273E-04	7.8125E-05	0.0417	0.0588	0.1005	0.5849
	t34-3	1421.1062	5.4818,	3.3203E-04	6.8359E-05	0.0523	0.0655	0.1178	0.5563
	t34-4	1040.1993	7.5477,	3.4180E-04	9.7656E-05	0.0333	0.0573	0.0905	0.6327
t35	t35-1	653.1484	1.6375,	3.1250E-04	1.0742E-04	0.0337	0.0285	0.0622	0.4583
	t35-2	1007.0704	3.5819,	3.7109E-04	9.7656E-05	0.0365	0.0520	0.0885	0.5881
	t35-3	1087.1947	5.6950,	2.8320E-04	8.7891E-05	0.0379	0.0528	0.0907	0.5820
	t35-4	1179.5697	7.7668,	3.6133E-04	1.1719E-04	0.0431	0.0597	0.1027	0.5806
t36	t36-1	1326.7961	1.4267,	3.1250E-04	9.7656E-05	0.0430	0.0673	0.1103	0.6105
	t36-2	847.6040	3.4638,	3.5156E-04	9.7656E-05	0.0307	0.0473	0.0780	0.6060
	t36-3	1118.3441	5.5012,	3.5156E-04	9.7656E-05	0.0424	0.0556	0.0979	0.5674
	t36-4	1088.7466	7.6297,	2.8320E-04	7.8125E-05	0.0331	0.0625	0.0955	0.6539
t37	t37-1	847.1194	1.6850,	3.2227E-04	9.7656E-05	0.0355	0.0409	0.0765	0.5352

	t37-2	711.2614	3.7576,	3.3203E-04	9.7656E-05	0.0314	0.0362	0.0677	0.5355
	t37-3	1016.0766	5.8042,	3.6133E-04	1.0742E-04	0.0426	0.0489	0.0915	0.5342
	t37-4	1054.9592	7.6913,	3.2227E-04	7.8125E-05	0.0401	0.0514	0.0916	0.5617
t38	t38-1	1169.0798	1.0309,	3.7109E-04	9.7656E-05	0.0390	0.0607	0.0997	0.6088
	t38-2	797.3251	2.8007,	3.1250E-04	8.7891E-05	0.0259	0.0459	0.0718	0.6389
	t38-3	1117.8867	4.6323,	3.1250E-04	6.8359E-05	0.0409	0.0556	0.0965	0.5762
	t38-4	1460.2812	6.4156,	3.2227E-04	8.7891E-05	0.0453	0.0757	0.1210	0.6258
t39	t39-1	609.7022	1.6497,	3.6133E-04	7.8125E-05	0.0236	0.0345	0.0581	0.5943
	t39-2	982.9530	3.4872,	2.7344E-04	8.7891E-05	0.0372	0.0464	0.0835	0.5550
	t39-3	893.5263	5.6517,	3.0273E-04	6.8359E-05	0.0309	0.0426	0.0735	0.5797
	t39-4	945.4669	7.5167,	3.1250E-04	9.7656E-05	0.0293	0.0581	0.0874	0.6643
t40	t40-1	1323.7328	1.6246,	3.5156E-04	1.0742E-04	0.0401	0.0709	0.1111	0.6388
	t40-2	983.1701	3.6327,	3.0273E-04	8.7891E-05	0.0361	0.0500	0.0861	0.5806
	t40-3	979.7425	5.5451,	3.1250E-04	7.8125E-05	0.0358	0.0504	0.0862	0.5850
	t40-4	629.7340	7.4474,	2.9297E-04	6.8359E-05	0.0213	0.0374	0.0587	0.6372
t41	t41-1	635.3174	1.8882,	2.7344E-04	5.8594E-05	0.0181	0.0411	0.0592	0.6943
	t41-2	853.7480	3.8229,	2.6367E-04	5.8594E-05	0.0202	0.0574	0.0775	0.7398
	t41-3	862.7358	5.7132,	3.2227E-04	6.8359E-05	0.0240	0.0572	0.0812	0.7049
	t41-4	898.6731	7.5024,	3.1250E-04	8.7891E-05	0.0314	0.0476	0.0789	0.6024
t42	t42-1	815.7137	1.8597,	3.6133E-04	6.8359E-05	0.0202	0.0563	0.0765	0.7364
	t42-2	1073.4142	3.4731,	3.0273E-04	6.8359E-05	0.0323	0.0650	0.0973	0.6679
	t42-3	1018.8327	5.2159,	3.0273E-04	5.8594E-05	0.0251	0.0664	0.0916	0.7256
	t42-4	833.5352	6.7748,	2.6367E-04	6.8359E-05	0.0270	0.0490	0.0760	0.6452
t43	t43-1	523.2624	1.7250,	3.3203E-04	6.8359E-05	0.0161	0.0336	0.0496	0.6761
	t43-2	693.2358	3.3249,	4.1016E-04	8.7891E-05	0.0218	0.0448	0.0666	0.6725
	t43-3	716.7113	5.1537,	3.0273E-04	6.8359E-05	0.0244	0.0428	0.0672	0.6366
	t43-4	669.0063	7.1090,	3.3203E-04	7.8125E-05	0.0228	0.0414	0.0642	0.6449
t44	t44-1	802.9767	1.8894,	3.3203E-04	6.8359E-05	0.0189	0.0566	0.0755	0.7493
	t44-2	875.9919	3.5354,	2.9297E-04	6.8359E-05	0.0274	0.0519	0.0793	0.6540
	t44-3	789.9585	5.4437,	3.1250E-04	6.8359E-05	0.0204	0.0518	0.0722	0.7173

	t44-4	1161.5768	7.4927,	2.7344E-04	5.8594E-05	0.0294	0.0732	0.1026	0.7132
t45	t45-1	706.9434	1.7186,	3.1250E-04	6.8359E-05	0.0238	0.0431	0.0669	0.6445
	t45-2	962.1737	3.7328,	2.8320E-04	5.8594E-05	0.0210	0.0650	0.0860	0.7554
	t45-3	424.5245	6.0710,	3.4180E-04	6.8359E-05	0.0114	0.0322	0.0436	0.7388
	t45-4	876.3953	8.1771,	3.4180E-04	5.8594E-05	0.0240	0.0584	0.0825	0.7084
t46	t46-1	540.1496	1.6133,	2.9297E-04	7.8125E-05	0.0182	0.0344	0.0526	0.6538
	t46-2	1327.8271	3.3766,	2.7344E-04	5.8594E-05	0.0336	0.0810	0.1146	0.7071
	t46-3	871.8068	5.4335,	4.2969E-04	1.7578E-04	0.0204	0.0608	0.0812	0.7489
	t46-4	866.7769	7.2946,	2.6367E-04	5.8594E-05	0.0220	0.0577	0.0797	0.7244
t47	t47-1	888.2129	1.2447,	2.5391E-04	8.7891E-05	0.0249	0.0446	0.0695	0.6419
	t47-2	803.4708	3.0027,	3.2227E-04	6.8359E-05	0.0231	0.0520	0.0752	0.6924
	t47-3	713.7636	4.7128,	2.7344E-04	6.8359E-05	0.0230	0.0433	0.0663	0.6534
	t47-4	886.2090	6.5645,	2.9297E-04	5.8594E-05	0.0222	0.0593	0.0815	0.7280
t48	t48-1	943.6830	1.8533,	2.8320E-04	7.8125E-05	0.0233	0.0601	0.0833	0.7208
	t48-2	843.6223	3.8236,	2.8320E-04	6.8359E-05	0.0256	0.0492	0.0748	0.6579
	t48-3	976.7740	5.8872,	3.0273E-04	5.8594E-05	0.0227	0.0641	0.0868	0.7381
	t48-4	992.1265	7.9394,	2.8320E-04	6.8359E-05	0.0214	0.0574	0.0788	0.7288
t49	t49-1	591.4352	1.5167,	3.1250E-04	5.8594E-05	0.0154	0.0419	0.0573	0.7306
	t49-2	600.3068	3.4808,	2.8320E-04	7.8125E-05	0.0166	0.0406	0.0572	0.7106
	t49-3	648.9348	5.5055,	2.9297E-04	6.8359E-05	0.0182	0.0443	0.0625	0.7086
	t49-4	805.0933	7.5968,	4.7852E-04	5.8594E-05	0.0195	0.0612	0.0807	0.7584
t50	t50-1	952.0967	1.3901,	3.0273E-04	6.8359E-05	0.0291	0.0566	0.0857	0.6600
	t50-2	676.8760	3.6990,	2.7344E-04	6.8359E-05	0.0197	0.0432	0.0629	0.6863
	t50-3	754.3766	6.0559,	2.7344E-04	5.8594E-05	0.0249	0.0445	0.0694	0.6411
	t50-4	833.7625	8.4404,	2.6367E-04	5.8594E-05	0.0206	0.0539	0.0745	0.7239
t51	t51-1	943.7815	2.2014,	2.6367E-04	5.8594E-05	0.0252	0.0632	0.0884	0.7151
	t51-2	1042.9073	4.4103,	2.7344E-04	6.8359E-05	0.0312	0.0673	0.0985	0.6832
	t51-3	697.7745	6.4737,	2.0898E-03	7.8125E-05	0.0201	0.0494	0.0695	0.7107
	t51-4	1265.0800	8.4315,	2.9297E-04	6.8359E-05	0.0381	0.0755	0.1136	0.6647
t52	t52-1	888.7236	2.1620,	3.4180E-04	6.8359E-05	0.0273	0.0556	0.0829	0.6702

	t52-2	1085.0312	3.9674,	3.2227E-04	7.8125E-05	0.0365	0.0656	0.1021	0.6428
	t52-3	1220.9325	5.8080,	3.0273E-04	8.7891E-05	0.0385	0.0719	0.1104	0.6513
	t52-4	1230.5118	7.6575,	2.8320E-04	6.8359E-05	0.0309	0.0828	0.1137	0.7283
t53	t53-1	740.0604	1.7786,	3.1250E-04	8.7891E-05	0.0255	0.0492	0.0747	0.6592
	t53-2	1109.7893	3.8755,	3.0273E-04	7.8125E-05	0.0373	0.0685	0.1058	0.6478
	t53-3	1112.0334	6.0560,	3.0273E-04	7.8125E-05	0.0358	0.0692	0.1051	0.6589
	t53-4	1114.7854	8.0405,	2.7344E-04	5.8594E-05	0.0298	0.0762	0.1061	0.7187
t54	t54-1	607.7897	1.7559,	4.2969E-04	1.4648E-04	0.0299	0.0429	0.0728	0.5889
	t54-2	1438.1945	3.5648,	3.0273E-04	7.8125E-05	0.0400	0.0943	0.1343	0.7021
	t54-3	1079.2634	5.4218,	3.1250E-04	8.7891E-05	0.0372	0.0684	0.1056	0.6479
	t54-4	1270.1383	7.2162,	2.6367E-04	6.8359E-05	0.0399	0.0763	0.1162	0.6569
t55	t55-1	884.8570	2.4523,	3.0273E-04	8.7891E-05	0.0253	0.0605	0.0857	0.7054
	t55-2	871.1513	4.2742,	3.1250E-04	7.8125E-05	0.0240	0.0531	0.0771	0.6890
	t55-3	1178.0713	6.1562,	3.0273E-04	6.8359E-05	0.0300	0.0829	0.1129	0.7343
	t55-4	770.5068	7.9926,	6.8359E-04	4.1016E-04	0.0244	0.0533	0.0776	0.6860
t56	t56-1	1142.1049	2.0986,	2.8320E-04	7.8125E-05	0.0396	0.0661	0.1057	0.6255
	t56-2	1272.9098	3.7813,	3.8086E-04	7.8125E-05	0.0408	0.0855	0.1263	0.6767
	t56-3	1095.5122	5.6983,	3.1250E-04	7.8125E-05	0.0335	0.0730	0.1064	0.6855
	t56-4	1161.7191	7.5310,	7.9102E-04	5.7617E-04	0.0305	0.0761	0.1066	0.7140
t57	t57-1	759.0856	1.8429,	4.2969E-04	8.7891E-05	0.0265	0.0492	0.0757	0.6495
	t57-2	534.9548	3.6723,	3.5156E-04	7.8125E-05	0.0161	0.0406	0.0568	0.7162
	t57-3	832.0866	5.5732,	3.5156E-04	7.8125E-05	0.0266	0.0566	0.0832	0.6805
	t57-4	984.4622	7.3785,	3.0273E-04	7.8125E-05	0.0286	0.0633	0.0919	0.6883
t58	t58-1	760.4861	1.8906,	3.0273E-04	8.7891E-05	0.0258	0.0475	0.0733	0.6481
	t58-2	1054.2865	3.5675,	2.8320E-04	6.8359E-05	0.0326	0.0644	0.0971	0.6638
	t58-3	1146.0243	5.3181,	3.0273E-04	7.8125E-05	0.0363	0.0669	0.1032	0.6484
	t58-4	1004.1494	6.8814,	2.9297E-04	7.8125E-05	0.0334	0.0609	0.0944	0.6457
t59	t59-1	550.4841	2.0624,	3.3203E-04	8.7891E-05	0.0200	0.0336	0.0535	0.6272
	t59-2	879.9956	3.7347,	2.6367E-04	7.8125E-05	0.0295	0.0558	0.0852	0.6542
	t59-3	859.6577	5.5370,	3.6133E-04	8.7891E-05	0.0301	0.0549	0.0850	0.6463

	t59-4	944.7141	7.3244,	2.8320E-04	8.7891E-05	0.0265	0.0607	0.0872	0.6958
t60	t60-1	1263.7594	1.7298,	2.8320E-04	7.8125E-05	0.0435	0.0763	0.1198	0.6370
	t60-2	980.2100	3.4212,	3.6133E-04	7.8125E-05	0.0301	0.0684	0.0985	0.6946
	t60-3	914.3223	5.3300,	3.8086E-04	7.8125E-05	0.0253	0.0660	0.0912	0.7231
	t60-4	1022.2568	7.3392,	3.2227E-04	6.8359E-05	0.0250	0.0648	0.0898	0.7213

Reference

[1] Lee, Jung-Ryul, Chen Ciang Chia, and Churl-Won Kong. "Review of pyroshock wave measurement and simulation for space systems." *Measurement* 45, no. 4 (2012): 631-642.

[2] Alexander, J. Edward. "Shock response spectrum-a primer." *Sound & vibration* 43, no. 6 (2009): 6-15.

[3] Harris, Cyril M., and Allan G. Piersol. *Harris' shock and vibration handbook*. Vol. 5. New York: McGraw-Hill, 2002.

[4] Jonsson, Martin. "Development of a shock test facility for qualification of space equipment." *Department of Applied Mechanics, Göteborg, Sweden* (2012).

[5] Küçükbayram, Anıl İsmail. "Analysis and verification of a pyroshock test system." Master's thesis, Middle East Technical University, 2021.

[6] Kim, Mun-Guk, In-Gul Kim, Eun-Su Go, Min-Hyeok Jeon, Min-Song Kang, and Jeong-Su Choi. "A Simple Approximate Method for Predicting Impact Force History and Application to Pyroshock Simulation." In *Proceedings of the World Congress on Engineering*, vol. 2. 2018.

[7] Maggio, Lorenzo. "A method for the FRF estimation of an automotive transmission using experimental data from on-road vehicle tests." PhD diss., Politecnico di Torino, 2018.

[8] Hill, Brian James. "Common Flight Test Module for Multiple Harsh Environments." PhD diss., University of Cincinnati, 2008.